iScience

CellPress
OPEN ACCESS

Article

Prioritizing transcriptional factors in gene regulatory networks with PageRank

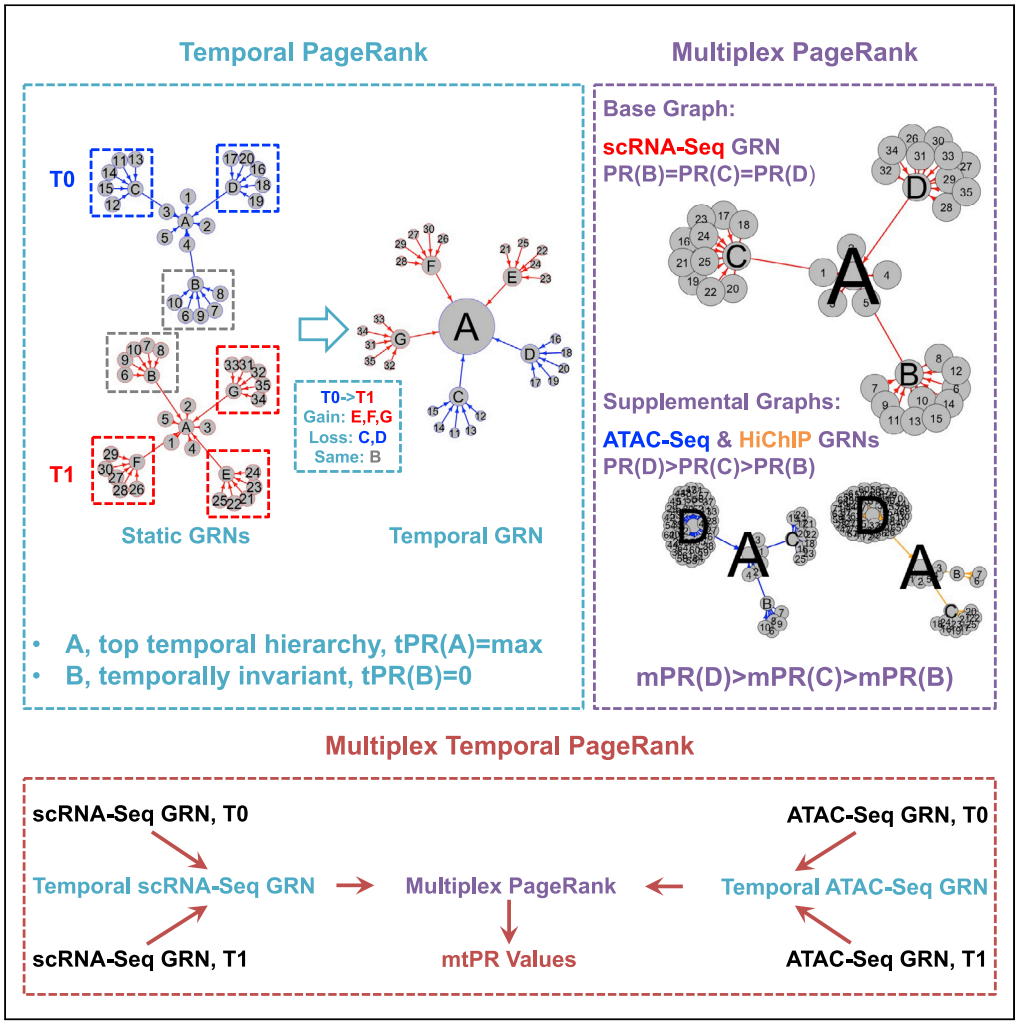

Hongxu Ding, Ying Yang, Yuanqing Xue, ..., Rojin Safavi, Andrea Califano, Joshua M. Stuart

hding16@ucsc.edu (H.D.)
jstuart@ucsc.edu (J.M.S.)

HIGHLIGHTS

Temporal PageRank prioritizes TFs controlling cellular state dynamics

Multiplex PageRank prioritizes TFs by integrating multi-omics GRNs

Temporal and multiplex PageRank can be used in combination for TF prioritization

Ding et al., iScience 24, 102017
January 22, 2021
https://doi.org/10.1016/j.isci.2020.102017

iScience

CellPress
OPEN ACCESS

Article

Prioritizing transcriptional factors in gene regulatory networks with PageRank

Hongxu Ding,[1,2,4,5,*] Ying Yang,[1,3,4] Yuanqing Xue,[1,4] Lucas Seninge,[1] Henry Gong,[1] Rojin Safavi,[1] Andrea Califano,[2] and Joshua M. Stuart[1,*]

SUMMARY

Biological states are controlled by orchestrated transcriptional factors (TFs) within gene regulatory networks. Here we show TFs responsible for the dynamic changes of biological states can be prioritized with temporal PageRank. We further show such TF prioritization can be extended by integrating gene regulatory networks reverse engineered from multi-omics profiles, e.g. gene expression, chromatin accessibility, and chromosome conformation assays, using multiplex PageRank.

INTRODUCTION

Biological processes are primarily executed via gene regulatory networks (GRNs), which are controlled by key transcriptional factors (TFs) (Levine and Davidson, 2005; Califano and Alvarez, 2017). Such key TFs usually occupy the top of the gene regulatory hierarchy (Chan and Kyba, 2013). The regulatory hierarchy of a specific TF depends on the number and hierarchy of corresponding transcriptional targets, thus can be quantified by PageRank centrality (Brin and Page, 1998; Page et al., 1999). Originally proposed for ranking search results of World Wide Web (WWW) snapshots, PageRank and related algorithms has been successfully applied to the analysis of single static biological networks (Morrison et al., 2005; Koschützki and Schreiber, 2008; Tarca et al., 2009; Iván and Grolmusz, 2011). The advent of high-throughput sequencing technologies provide unprecedented temporal and multi-dimensional biological information for understanding transcriptional regulation. For instance, transcriptional regulatory dynamics among consecutive biological states can be characterized with single cell RNA sequencing (scRNA-Seq) (Kolodziejczyk et al., 2015) and trajectory analysis (Herring et al., 2018). Meanwhile, epigenetic regulation of gene transcription can be illustrated using, e.g. chromatin accessibility (Klemm et al., 2019) and chromosome conformation (Sati and Cavalli, 2017) assays. Here, we show within such temporal and multiplex GRNs, TFs can be prioritized with temporal (Rozenshtein and Gionis, 2016) and multiplex (Halu et al., 2013) PageRank.

As the extension of original steady-state PageRank in temporal networks, temporal PageRank ranks nodes based on their connections that change over time (Rozenshtein and Gionis, 2016). In temporal GRNs, important TFs are those connected with more time-related targets and other important TFs. Such TFs will then be considered at the top of the temporal gene regulatory hierarchy and prioritized (Figure 1A, see Transparent methods). Multiplex PageRank, on the other hand, extends PageRank analysis to multiplex networks. In such networks, the same nodes might interact with one another in different layers. Multiplex PageRank is then calculated according to the topology of a predefined base network, with regular PageRank of other supplemental networks as edge weights and personalization vector (Halu et al., 2013). Therefore, GRNs reverse engineered from multi-omics assays can be integrated for TF prioritization (Figure 1B, see Transparent methods).

RESULTS

Interpreting regulatory dynamics using temporal PageRank

We first demonstrated TFs controlling cellular state transitions can be prioritized with temporal PageRank. Specifically, we analyzed the human myoblast-muscle cell differentiation process, during which single cells were harvested and profiled every 24 hr from T0 to T72 (Trapnell et al., 2014). To provide intuitions for the rationale of temporal PageRank analysis, following the schematic diagram in Figure 1A, we visualized static GRNs at neighboring timepoints, as well as the yielding temporal GRNs. Considering the sizes of such static/temporal GRNs, for clear visualization, we only highlighted key regulatory modules by filtering out less confident

[1]Department of Biomolecular Engineering and Genomics Institute, University of California, Santa Cruz, Santa Cruz, CA, USA

[2]Department of Systems Biology, Columbia University, New York, NY, USA

[3]Department of Dermatology, Stanford University, Stanford, CA, USA

[4]These authors contributed equally

[5]Lead Contact

*Correspondence: hding16@ucsc.edu (H.D.), jstuart@ucsc.edu (J.M.S.)

https://doi.org/10.1016/j.isci.2020.102017

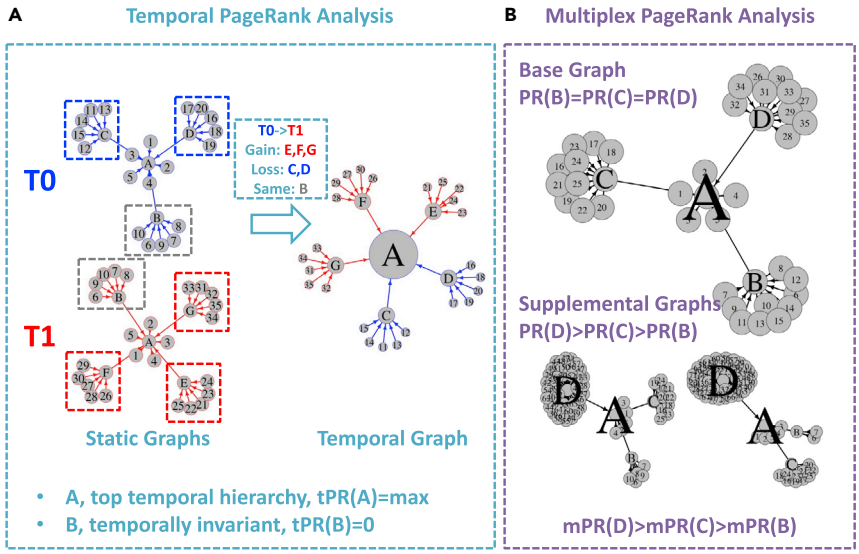

Figure 1. Graphic overview

Schematic diagrams of temporal and multiplex PageRank analysis are shown in (A) and (B), respectively.

interactions (see Transparent methods). As shown in Figure 2A, two independent regulatory modules were identified at T0. The first module was controlled by cell cycle TFs *TOP2A* (Mjelle et al., 2015) and *FOXM1* (Wierstra and Alves, 2007), in concordance with the active proliferation of myoblasts. The second module, which is responsible for the lineage identity of myoblast, was marked by the lineage-specific TF *MYF5* (Blais et al., 2005). As for T24 (Figure 2B) and the following timepoints (Figure S1), the corresponding GRNs were majorly controlled by a single regulatory module. Such a module was composed of muscle cell-specific TFs, including muscle cell lineage markers *MEF2C* and *ANKRD1* (Blais et al., 2005), as well as epigenetic modifier *HMGA1* (Brocher et al., 2010). Thus, the differentiation of myoblast can be described as the sequential interplay of key TFs. We further applied temporal PageRank on the differential GRNs derived from the corresponding adjacent static counterparts. As shown in Figures 2C and S1, the regulatory dynamics of myoblast-muscle cell differentiation was recapitulated, by discovering all the above-mentioned key TFs. We also analyzed the 33 major lineages during mouse organogenesis reported in the MOCA data sets (Cao et al., 2019) as the additional proof-of-concept (Figure S2).

Integrating multi-omics GRNs using multiplex PageRank

We then demonstrated GRNs reverse engineered from multi-omics assays can be integrated through multiplex PageRank for TF prioritization. Specifically, we included matching ATAC-Seq profiles (Pliner et al., 2018) of the above-mentioned differentiation process. We then constructed static and temporal GRNs, and performed corresponding PageRank analysis, following the workflow described in Transparent methods. Although the scRNA-Seq and ATAC-Seq GRNs were topologically different (Figure S1), muscle cell signature TF *MEF2C* was identified with both GRN types across the entire differentiation process (Figure S3). Meanwhile, additional muscle cell TFs, e.g. *KLF5* (Hayashi et al., 2016) and *REST* (Iannotti et al., 2013) were recapitulated by analyzing ATAC-Seq GRNs (Figure S3). Such results suggested GRNs reverse engineered from multi-omics profiles agreed on the general principle, while each provided unique insights into the gene regulatory machinery. Aiming at prioritizing TFs by combining scRNA-Seq and ATAC-Seq GRNs, we performed multiplex PageRank analysis. The contributions of scRNA-Seq and ATAC-Seq GRNs were quantified in Figures 2F and 2G. Noticeably, multiplex PageRank can be applied to integrate GRNs under both static and temporal scenarios. As shown in Figures 2D, 2E and S4, key TFs elucidated from scRNA-Seq and ATAC-Seq GRNs were together recapitulated.

As an additional proof-of-concept, we analyzed the human hematopoiesis process, including the linear lineage progression of hematopoietic stem cell, multi-potent progenitor, and CMP (common myeloid progenitor), as well as the bifurcation from CMP to granulocyte-macrophage progenitor and megakaryocyte-erythroid progenitor, with multiplex PageRank. Following the same pipeline as the previous analysis, GRNs assembled from matching scRNA-Seq (Pellin et al., 2019) and ATAC-Seq (Corces et al., 2016) data sets were analyzed (Figure S5).

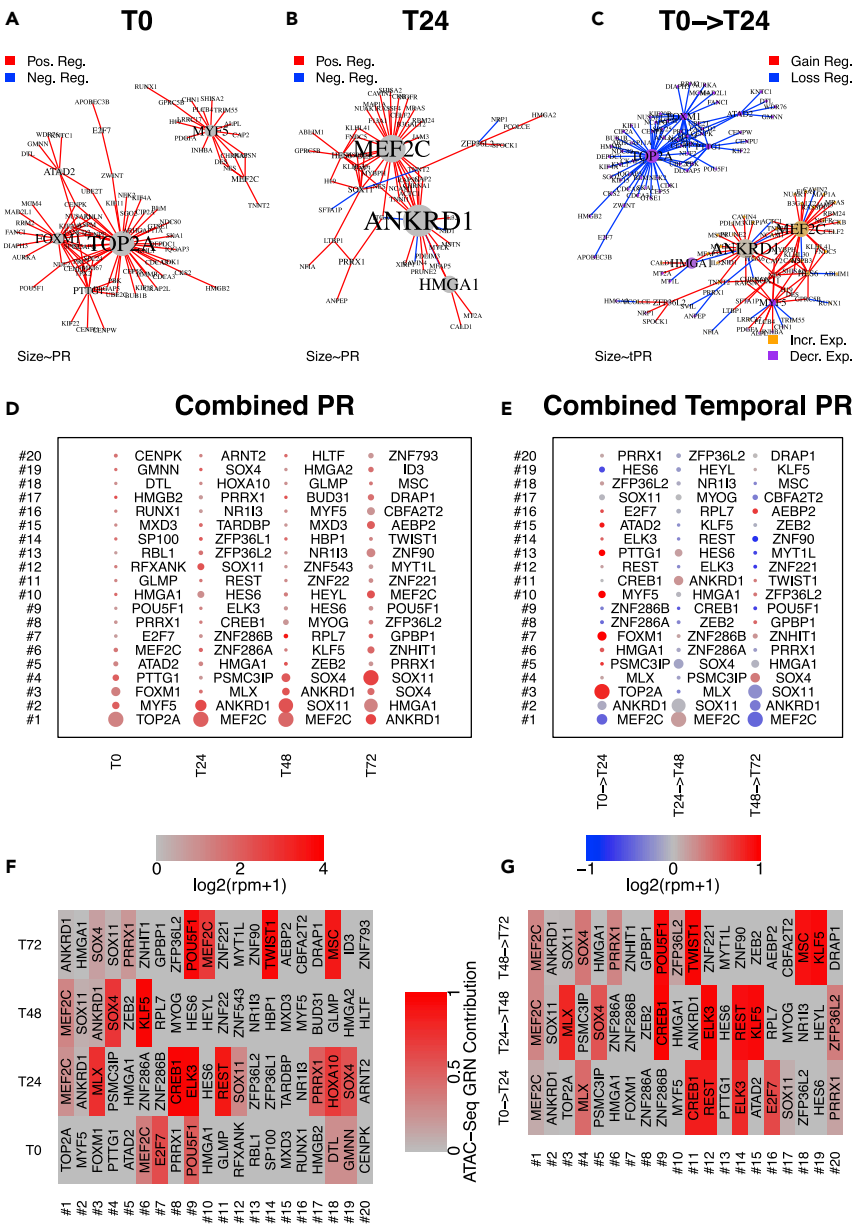

Figure 2. PageRank analysis on the myoblast-muscle cell differentiation process

(A and B) Static scRNA-Seq GRNs for T0 and T24. Vertex and label sizes correspond to static PageRank values. Red and blue edges correspond to positive and negative interactions, respectively.

(C) Temporal scRNA-Seq GRN between T0 and T24. Vertex and label sizes correspond to temporal PageRank values. Orange and purple vertices correspond to increased and decreased gene expression from T0 to T24, respectively. Red and blue edges correspond to gained and lost interactions from T0 to T24, respectively.

(D and E) Bubble plots showing the top 20 combined static and temporal PageRank candidates by analyzing scRNA-Seq and ATAC-Seq GRNs. The size of bubbles correspond to the degree values (number of connecting interactions). The color of bubbles correspond to the gene expression quantified by log2(rpm+1), where rpm stands for reads per million. For static PageRank, absolute gene expression was quantified, with red and gray corresponding to high and low gene expression, respectively. For temporal PageRank, differential gene expression was quantified, with red and blue corresponding to increased and decreased gene expression, respectively.

(F and G) Heatmaps showing the contribution of ATAC-Seq GRNs in TF prioritization. The contributions of scRNA-Seq and ATAC-Seq GRNs were normalized to 1. F and G describes static and temporal PageRank analysis, respectively.

We further expanded multiplex PageRank to integrate gene expression, chromatin accessibility and chromosome conformation GRNs, by analyzing scRNA-Seq, ATAC-Seq, and HiChIP (Mumbach et al., 2017) profiles of human T-cells. We used scRNA-Seq GRN as the base network for the integration. As shown in Figure S6, several known crucial TFs responsible for T cell homeostasis, e.g. *FOXP1* (Feng et al., 2011) and functionalities, e.g. *LEF1* (Travis et al., 1991) were recapitulated among the top 20 identified TFs. Moreover, a systematic survey of the top 20 TFs was performed with GO analysis (http://geneontology.org/). As shown in Table S1, a significant amount of T-cell-related biological processes were recapitulated. Noticeably, the three included GRNs complement each other by providing unique insights into gene regulatory machinery. For instance, the prioritization of *LEF1* and *FOXP1* was majorly contributed by the HiChIP and ATAC-Seq GRNs, respectively.

DISCUSSION

Taken together, by analyzing diverse biological questions, we demonstrated that key TFs responsible for biological processes can be prioritized by analyzing GRNs using PageRank. Specifically, we showed that the crucial TFs controlling the dynamic transition of biological states can be prioritized with temporal PageRank. Further, we showed GRNs reverse engineered from multi-omics profiles can be integrated for TF prioritization with multiplex PageRank.

PageRank quantifies the importance of TFs during biological processes by performing comprehensive surveys on GRN hierarchies, therefore extremely suitable for TF prioritization. Specifically, PageRank analysis can prioritize TFs even if their expression patterns are obscure. For instance, as shown in Figure 2E, although no strong differential expression was observed during the transition from T0 to T24, muscle cell-specific TF *ANKRD1* was ranked #2 with temporal PageRank analysis. Meanwhile, PageRank analysis prioritizes TFs with the entire GRN hierarchies, rather than based on "flattened" architectures which only consider the direct targets. For instance, as shown in Figure S2, during the mouse embryo development of inhibitory interneuron lineage from stage E10.5 to stage E11.5, the degree centrality of *Sox6* was insignificant, while ranked #3 by temporal PageRank analysis. We further performed a systematic comparison between our PageRank analysis with a state-of-the-art TF prioritization algorithm, VIPER (Alvarez et al., 2016; Ding et al., 2018) (see Figure S11 for details).

Limitations of the study

Taken together, we anticipate the PageRank analysis would provide novel and comprehensive insights for the understanding of transcriptional regulation, by identifying regulators that potentially reside at the top of the regulatory hierarchy. One thing to be noticed for temporal PageRank analysis is that, we would not recommend applying it on distinct networks. Consider an extreme case, where (1) the number of nodes in network A and B are the same, while A has 10 times more interactions than B, and (2) the two networks have no overlapping interactions, for example. The differential network between A and B will include all interactions in A and B. If temporal PageRank analysis is performed on such a differential network, the yielded top ranks will be dominated by A nodes, considering the 10 times more interactions. B nodes, on the other hand, are under-appreciated even though they also convey important information describing differences between A and B. As for analyzing GRNs, similar biases could happen. For instance, the epigenetic landscape of zygotes is less restricted, thus more regulatory interactions are expected. In contrast, the more restricted epigenetic landscapes reduce possible regulatory interactions in terminally differentiated cells such as T-cells. Thus, the temporal PageRank analysis between zygote and T cell GRNs is highly likely to ignore functional TFs in T-cells. We thus would suggest only applying temporal PageRank analysis between temporally adjacent networks.

As for multiplex PageRank analysis, one limitation is that the results might vary according to the choice of the base network. For instance, during the myoblast-muscle cell differentiation process, although known myoblast-specific TFs *SP1/3* (Parakati and DiMario, 2002) were prioritized by PageRank analyses based on only ATAC-Seq GRNs (Figure S3), they failed to be captured when using scRNA-Seq GRNs as base networks for multiplex PageRank analyses (Figures 2D and 2E). On the other hand, the effect of base network choice on the final multiplex PageRank integration was minor when analyzing T-cells (Figure S7). Thus, one possible future direction might be developing "reciprocal" multiplex PageRank analysis for GRNs, in which feedbacks among multiplex networks are considered as reported in (Tu et al., 2018).

Resource availability

Lead contact

Hongxu Ding, hding16@ucsc.edu.

Material availability

This study did not generate any new material.

Data and code availability

scRNA-Seq profiles of myoblast-muscle cell differentiation were downloaded from Gene Expression Omnibus (GEO) under accession number GSE52529. MOCA scRNA-Seq profiles were downloaded from GEO under accession number GSE119945. Hematopoiesis scRNA-Seq profiles were downloaded from GEO under accession number GSE117498. Healthy PBMC T cell scRNA-Seq profiles were downloaded from: https://support.10xgenomics.com/single-cell-gene-expression/datasets/3.0.0/pbmc_10k_v3. ATAC-Seq profiles of myoblast-muscle cell differentiation were downloaded from GEO under accession number GSE109828. Hematopoiesis ATAC-Seq profiles were downloaded from GEO under accession number GSE74912. T cell ATAC-Seq and Hi-ChIP profiles were downloaded from GEO under accession number GSE101498.

The pageRank R package is available on Bioconductor, and GitHub repository https://github.com/hd2326/pageRank. Custom scripts used to reproduce the results and figures are also available at https://github.com/hd2326/pageRank.

METHODS

All methods can be found in the accompanying Transparent Methods supplemental file.

SUPPLEMENTAL INFORMATION

Supplemental Information can be found online at https://doi.org/10.1016/j.isci.2020.102017.

ACKNOWLEDGMENTS

J.M.S. was supported by a grant 5R01GM109031 from the NIGMS. J.M.S. and H.D. were supported by a grant from the Chan Zuckerberg Initiative's Human Cell Atlas portals project. H.D. was supported by a gift from Seagate Technology. J.M.S. was supported by grant GC1R-06673-C from the California Institute for Regenerative Medicine's Center of Excellence for Stem Cell Genomics.

AUTHOR CONTRIBUTIONS

H.D. conceived the idea. H.D. and A.C. performed ARACNe analysis. H.D. and Y.Y. performed epigenetic network analysis. H.D., Y.Y., Y.X., H.G., and R.S. performed the PageRank analysis. H.D., Y.Y., Y.X., and L.S. collected and pre-processed the data. H.D. and J.M.S. supervised the project. H.D., Y.Y. and J.M.S. wrote the manuscript.

DECLARATION OF INTERESTS

The authors declare no competing interests.

Received: October 6, 2020
Revised: November 6, 2020
Accepted: December 28, 2020
Published: January 22, 2021

REFERENCES

Alvarez, M.J., Shen, Y., Giorgi, F.M., Lachmann, A., Ding, B.B., Ye, B.H., and Califano, A. (2016). Functional characterization of somatic mutations in cancer using network-based inference of protein activity. Nat. Genet. *48*, 838–847.

Blais, A., Tsikitis, M., Acosta-Alvear, D., Sharan, R., Kluger, Y., and Dynlacht, B.D. (2005). An initial blueprint for myogenic differentiation. Genes Dev. *19*, 553–569.

Brin, S., and Page, L. (1998). The anatomy of a large-scale hypertextual web search engine. Comput. Netw. *30*, 107–117.

Brocher, J., Vogel, B., and Hock, R. (2010). HMGA1 down-regulation is crucial for chromatin composition and a gene expression profile permitting myogenic differentiation. BMC Cell. Biol. *11*, 1–12.

Califano, A., and Alvarez, M.J. (2017). The recurrent architecture of tumour initiation, progression and drug sensitivity. Nat. Rev. Cancer *17*, 116.

Cao, J., Spielmann, M., Qiu, X., Huang, X., Ibrahim, D.M., Hill, A.J., Zhang, F., Mundlos, S., Christiansen, L., Steemers, F.J., and Trapnell, C. (2019). The single-cell transcriptional landscape of mammalian organogenesis. Nature *566*, 496–502.

Chan, S.S.K., and Kyba, M. (2013). What is a master regulator? J. Stem Cell Res. Ther. *3*, https://doi.org/10.4172/2157-7633.1000e114.

Corces, M.R., Buenrostro, J.D., Wu, B., Greenside, P.G., Chan, S.M., Koenig, J.L., Snyder, M.P., Pritchard, J.K., Kundaje, A., Greenleaf, W.J., and Majeti, R. (2016). Lineage-specific and single-cell chromatin accessibility charts human

hematopoiesis and leukemia evolution. Nat. Genet. *48*, 1193–1203.

Ding, H., Douglass, E.F., Sonabend, A.M., Mela, A., Bose, S., Gonzalez, C., Canoll, P.D., Sims, P.A., Alvarez, M.J., and Califano, A. (2018). Quantitative assessment of protein activity in orphan tissues and single cells using the metaVIPER algorithm. Nat. Commun. *9*, 1–10.

Feng, X., Wang, H., Takata, H., Day, T.J., Willen, J., and Hu, H. (2011). Transcription factor Foxp1 exerts essential cell-intrinsic regulation of the quiescence of naive T cells. Nat. Immunol. *12*, 544–550.

Halu, A., Mondragón, R.J., Panzarasa, P., and Bianconi, G. (2013). Multiplex pagerank. PLoS One *8*, e78293.

Hayashi, S., Manabe, I., Suzuki, Y., Relaix, F., and Oishi, Y. (2016). Klf5 regulates muscle differentiation by directly targeting muscle-specific genes in cooperation with MyoD in mice. Elife *5*, e17462.

Herring, C.A., Chen, B., McKinley, E.T., and Lau, K.S. (2018). Single-cell computational strategies for lineage reconstruction in tissue systems. Cell Mol. Gastroenterol. Hepatol. *5*, 539–548.

Iannotti, F.A., Barrese, V., Formisano, L., Miceli, F., and Taglialatela, M. (2013). Specification of skeletal muscle differentiation by repressor element-1 silencing transcription factor (REST)-regulated Kv7. 4 potassium channels. Mol. Biol. Cell *24*, 274–284.

Iván, G., and Grolmusz, V. (2011). When the Web meets the cell: using personalized PageRank for analyzing protein interaction networks. Bioinformatics *27*, 405–407.

Klemm, S.L., Shipony, Z., and Greenleaf, W.J. (2019). Chromatin accessibility and the regulatory epigenome. Nat. Rev. Genet. *20*, 207–220.

Kolodziejczyk, A.A., Kim, J.K., Svensson, V., Marioni, J.C., and Teichmann, S.A. (2015). The technology and biology of single-cell RNA sequencing. Mol. Cell *58*, 610–620.

Koschützki, D., and Schreiber, F. (2008). Centrality analysis methods for biological networks and their application to gene regulatory networks. Gene Regul. Syst. Biol. *2*, GRSB-S702.

Levine, M., and Davidson, E.H. (2005). Gene regulatory networks for development. Proc. Natl. Acad. Sci. U S A *102*, 4936–4942.

Mjelle, R., Hegre, S.A., Aas, P.A., Slupphaug, G., Drabløs, F., Sætrom, P., and Krokan, H.E. (2015). Cell cycle regulation of human DNA repair and chromatin remodeling genes. DNA Repair *30*, 53–67.

Morrison, J.L., Breitling, R., Higham, D.J., and Gilbert, D.R. (2005). GeneRank: using search engine technology for the analysis of microarray experiments. BMC Bioinformatics *6*, 233.

Mumbach, M.R., Satpathy, A.T., Boyle, E.A., Dai, C., Gowen, B.G., Cho, S.W., Nguyen, M.L., Rubin, A.J., Granja, J.M., Kazane, K.R., and Wei, Y. (2017). Enhancer connectome in primary human cells identifies target genes of disease-associated DNA elements. Nat. Genet. *49*, 1602.

Page, L., Brin, S., Motwani, R., and Winograd, T. (1999). The PageRank Citation Ranking: Bringing Order to the Web (Stanford InfoLab).

Parakati, R., and DiMario, J.X. (2002). Sp1-and Sp3-mediated transcriptional regulation of the fibroblast growth factor receptor 1 gene in chicken skeletal muscle cells. J. Biol. Chem. *277*, 9278–9285.

Pellin, D., Loperfido, M., Baricordi, C., Wolock, S.L., Montepeloso, A., Weinberg, O.K., Biffi, A., Klein, A.M., and Biasco, L. (2019). A comprehensive single cell transcriptional landscape of human hematopoietic progenitors. Nat. Commun. *10*, 1–15.

Pliner, H.A., Packer, J.S., McFaline-Figueroa, J.L., Cusanovich, D.A., Daza, R.M., Aghamirzaie, D., Srivatsan, S., Qiu, X., Jackson, D., Minkina, A., and Adey, A.C. (2018). Cicero predicts cis-regulatory DNA interactions from single-cell chromatin accessibility data. Mol. Cell *71*, 858–871.

Rozenshtein, P., and Gionis, A. (2016). September. Temporal pagerank. In Joint European Conference on Machine Learning and Knowledge Discovery in Databases (Springer), pp. 674–689.

Sati, S., and Cavalli, G. (2017). Chromosome conformation capture technologies and their impact in understanding genome function. Chromosoma *126*, 33–44.

Tarca, A.L., Draghici, S., Khatri, P., Hassan, S.S., Mittal, P., Kim, J.S., Kim, C.J., Kusanovic, J.P., and Romero, R. (2009). A novel signaling pathway impact analysis. Bioinformatics *25*, 75–82.

Trapnell, C., Cacchiarelli, D., Grimsby, J., Pokharel, P., Li, S., Morse, M., Lennon, N.J., Livak, K.J., Mikkelsen, T.S., and Rinn, J.L. (2014). The dynamics and regulators of cell fate decisions are revealed by pseudotemporal ordering of single cells. Nat. Biotechnol. *32*, 381.

Travis, A., Amsterdam, A., Belanger, C., and Grosschedl, R. (1991). LEF-1, a gene encoding a lymphoid-specific protein with an HMG domain, regulates T-cell receptor alpha enhancer function [corrected]. Genes Dev. *5*, 880–894.

Tu, X., Jiang, G.P., Song, Y., and Zhang, X. (2018). Novel multiplex PageRank in multilayer networks. IEEE Access *6*, 12530–12538.

Wierstra, I., and Alves, J. (2007). FOXM1, a typical proliferation-associated transcription factor. Biol. Chem. *388*, 1257–1274.

iScience, Volume *24*

Supplemental Information

Prioritizing transcriptional factors in gene regulatory networks with PageRank

Hongxu Ding, Ying Yang, Yuanqing Xue, Lucas Seninge, Henry Gong, Rojin Safavi, Andrea Califano, and Joshua M. Stuart

Supplemental Data Items

Figure S1. [Graph visualization of myoblast-muscle cell differentiation GRNs], related to Figure 2. (A) Static scRNA-Seq GRNs. Bigger vertices corresponded to higher regular PageRank values. Red/blue edges corresponded to positive/negative interactions, respectively. (B) Static ATAC-Seq GRNs. Bigger vertices corresponded to higher regular PageRank values. (C, D) Temporal scRNA-Seq and ATAC-Seq GRNs. Bigger vertices corresponded to higher temporal PageRank values. Orange/purple vertices corresponded to increased/decreased gene expression, respectively. Red/blue edges corresponded to gained/lost interactions, respectively. T0, T24, T48 and T72 corresponded to sampling timepoints alongside the differentiation process as reported in [1].

Figure S2. [Static PageRank analysis on MOCA lineages], related to Figure 2. We analyzed mouse organogenesis lineages reported in the MOCA datasets [2]. For every lineage, the top 20 static and temporal PageRank (the left and right panels of every lineage) candidates were shown in bubble plots. The size of bubbles corresponded to the degree: the more connecting interactions the bigger the bubble. The color of bubbles corresponded to the gene expression. For static PageRank panels, red/grey corresponded to high/low gene expression, respectively. For temporal PageRank panels, reg/blue corresponded to increased/decreased gene expression, respectively. E9.5 etc, embryonic stages.

Figure S3. [Static and temporal PageRank analysis on myoblast-muscle cell differentiation], related to Figure 2. The top 20 static and temporal PageRank candidates by analyzing scRNA-Seq [1] and ATAC-Seq [3] GRNs were shown in bubble plots. The size of bubbles corresponded to the degree: the more connecting interactions the bigger the bubble. The color of bubbles corresponded to the gene expression. For static PageRank analysis, red/grey corresponded to high/low gene expression, respectively. For temporal PageRank analysis, red/blue corresponded to increased/decreased gene expression, respectively. PR, static PageRank; tPR, temporal PageRank; T0 etc, differentiation timepoints.

Figure S4. [Multiplex PageRank analysis on myoblast-muscle cell differentiation], related to Figure 2. The top 20 multiplex (additive, multiplicative, combined and neutral, see METHODS for details) PageRank candidates by combining scRNA-Seq [1] and ATAC-Seq [3] GRNs were shown in bubble plots. The size of bubbles corresponded to the degree: the more connecting interactions the bigger the bubble. The color of bubbles corresponded to the gene expression. For static PageRank analysis, red/grey corresponded to high/low gene expression, respectively. For temporal PageRank analysis, reg/blue corresponded to increased/decreased gene expression, respectively. PR, static PageRank; tPR, temporal PageRank; T0 etc, differentiation timepoints.

Figure S5. [Multiplex PageRank analysis on hematopoiesis], related to Figure 2. The top 20 multiplex (additive, multiplicative, combined and neutral, see METHODS for details) PageRank candidates by combining scRNA-Seq [4] and ATAC-Seq [5] GRNs were shown in bubble plots. The size of bubbles corresponded to the degree: the more connecting interactions the bigger the bubble. The color of bubbles corresponded to the gene expression. For static PageRank analysis, red/grey corresponded to high/low gene expression, respectively. For temporal PageRank analysis, reg/blue corresponded to increased/decreased gene expression, respectively. PR, static PageRank; tPR, temporal PageRank; T0 etc, differentiation timepoints.

Figure S6. [PageRank analysis on T-cells], related to Figure 2. (A) Static PageRank values calculated from scRNA-Seq, ATAC-Seq and HiChIP GRNs reverse engineered from healthy human T-cells were analyzed [6]. The size of points correspond to the combined static PageRank values, and the color of points correspond to whether they are TFs or targets. (B) Top 20 combined static PageRank candidates. The contributions of each GRN were represented as normalized fractions. Red green and blue correspond to scRNA-Seq, ATAC-Seq and HiChIP GRNs, respectively.

Figure S7. [Effect of base network on multiplex PageRank], related to Figure 2. The scRNA-Seq, ATAC-Seq and HiChIP static GRNs reverse engineered from healthy human T-cells were analyzed [6]. (A) Multiplex PageRank values calculated from different base GRNs. (B) Scatter plot of regular versus multiplex (additive, multiplicative, combined and neutral, see METHODS for details) PageRank values calculated from different base GRNs.

Figure S8. [Overview of the analytical workflow], related to Figure 2.

Figure S9. [Overview of epigenetic GRN construction], related to Figure 2.

Figure S10. [Complexity analysis], related to Figure 2. We generated 10 random Erdos-Renyi graphs, represented as ER(n, p), per n-p combination to gain enough statistical power for complexity analysis. Specifically, log2(n) ranges from 5 to 14, while p equals 0.1. For both multiplex and temporal PageRank analyses, the complexity scales exponentially with the network size. Noticeably, even the largest ER graphs, which contain 2^14 (16384) nodes, can be processed within 2 hours, suggesting the decent efficiency of our temporal and multiplex PageRank implementations.

Figure S11. [Systematic comparison with state-of-the-art TF prioritization algorithm VIPER], related to Figure 2. Enrichment analysis-based algorithms, e.g. VIPER [7] and successor metaVIPER [8], as well as SCENIC [9], emerged as powerful tools for prioritizing TFs from GRNs. Such algorithms evaluate the activity of TFs by enriching the gene expression signatures against the corresponding transcriptional targets. If a majority of positive/negative targets of a specific TF are over/under-expressed, then such a TF can be considered as activated, and vice versa. With the quantified enrichment score, TFs can be prioritized. Specifically, we chose the VIPER algorithm for comparison study. VIPER has successfully prioritized TFs in various biological conditions, thus can be considered as the “ground truth” algorithm. For systematic comparison, we analyzed all the 33 MOCA lineages [2] using the VIPER algorithm [8,9]. We further compared the VIPER-inferred TF activities with temporal PageRank values, as described in Figure S2. The x-axis denotes the normalized enrichment score (nES, TF activity) quantified by VIPER, and the y-axis denotes the temporal PageRank values. The colored dots represent TFs during different developmental transitions. As shown, in general PageRank values agree with VIPER inferences, suggesting the recapitulation of key TFs. However, there were cases where discrepancies between the PageRank values and nES scores. VIPER evaluates TF activities by only visiting their direct transcriptional targets, thus cannot fully appreciate the hierarchy of gene regulatory networks. PageRank, on the other hand, performs a comprehensive survey on the network topology for systematic evaluation of the importance of TFs. For instance, during the E12.5-E13.5 development of mouse radial glia, *Whsc1* regulates *Tcf12* and *Pax3* (purple). As shown in panel “Radial-glia”, the moderate differential expression of *Tcf12* and *Pax3* gave less significant VIPER nES. In contrast, the PageRank value of *Tcf12* ranked #1 among all TFs, thus significantly promoted the importance of *Whsc1*. Such a dissection of the *Whsc1* sub-network provides a good example of the advantage of PageRank analysis.

Table S1. [Result of the T-cell GO analysis], related to Figure 2. Results of online GO analysis (http://geneontology.org/) with the top 20 identified TFs reported in Figure S6.

Transparent Methods

Overview of the analytical workflow.

As shown in Figure S8, cell type-specific TF-target networks will first be constructed from corresponding multi-omics profiles (see subsections “Gene expression-based GRNs” and “Epigenetic GRNs” for details). TF-target interactions will then be filtered based on confidence scores derived from the expression of TFs and corresponding targets. The confidence scores were calculated based on marginal and joint expression distribution, using either their differences or mutual information. Based on the null model calculated from random TF-target pairs, interactions with p-value smaller than 10^{-3} were kept for downstream analysis. Such filtered GRNs can then be used to generate temporal GRNs, followed by temporal PageRank analysis (see section “temporal PageRank” for details). Such steady-state and temporal GRNs can be cleaned by removing certain nodes, further adjusted by user-provided edge weights, personalization vectors and damping factors. Finally, multiplex PageRank can be calculated among such filtered and adjusted GRNs (see section “multiplex PageRank” for details).

Gene expression-based GRNs.

GRNs are conventionally reverse engineered from expression profiles [10]. Several well-established algorithms have been proposed to construct expression-based tissue-specific GRNs, as reviewed in [11]. Here, we specifically chose the ARACNe algorithm, considering the superior accuracy [12-14]. ARACNe was run on scRNA-Seq profiles with 200 bootstrap iterations using 1813 transcription factors (genes annotated in gene ontology molecular function database, as GO:0003700, “transcription factor activity”, or as GO:0003677, “DNA binding”, and GO:0030528, “transcription regulator activity”, or as GO:00034677 and GO: 0045449, “regulation of transcription”). Parameters were set to zero DPI (Data Processing Inequality) tolerance and MI (Mutual Information) p-value (using MI computed by permuting the original dataset as null model) threshold of 10^{-8}. The ARACNe algorithm is available at https://github.com/califano-lab/ARACNe-AP.

Epigenetic GRNs.

In this study we focused on chromatin accessibility and chromosome conformation epigenetic assays. Chromatin accessibility assays, e.g. DNase-Seq [15,16], MNase-Seq [17], NOMe-Seq [18], ATAC-Seq [19] and derivatives are designed to identify physically accessible DNA regions, which are likely to be involved in transcriptional regulation. As shown in Figure S9, motif searching will be performed within called peaks (accessible regions) to identify putative TFs. Meanwhile, TSSs (Transcription Start Sets) will be searched within certain upstream and downstream genomic ranges of peaks to identify potential target genes. Thus, TF-target can be corresponded for GRNs assembly.

Chromosome conformation assays, e.g. ChIA-PET [20], 3C [21], 4C [22], 5C [23], Hi-C [24], HiChIP [6] and derivatives are designed to map spatial organization of chromosomes. Such spatial organization usually results in transcriptional regulation. As shown in Figure S9, chemical crosslink will preserve long-range interactions of genomic regions. Within such regions, TF binding motifs and TSSs will be searched for GRNs assembly, as described before.

Specifically, for TSS searching, genes will first be retrieved from Bioconductor R TxDb annotations [25] using the function genes in Bioconductor R package GenomicFeatures [26]. Then the corresponding promoter regions will be determined using the function promoters in Bioconductor R package GenomicRanges [26]. For motif searching, the most updated JASPAR database (available in Bioconductor R package JASPAR2018) [27] will be searched using the function getMatrixSet in Bioconductor R package TFBSTools [28]. Then functions matchMotifs and motifMatches in Bioconductor R package motifmatchr [29] will be used to match motifs to TFs.

Temporal PageRank.

Temporal PageRank extends the original static PageRank by only considering temporal edges instead of all edges. Temporal edges denote edges that change at certain stages during the lifetime of the networks [30]. Here, we simplify the definition of temporal PageRank by examining GRN pairs describing consecutive biological states, e.g. T0 and T24 of myoblast-muscle differentiation. Thus, we represented such GRN pairs using adjacency matrices, then took the subtraction as representation of temporal differential networks, further for temporal PageRank calculation. We implemented temporal PageRank as the function diff_graph in R package pageRank, based on CRAN R package igraph [31]. As shown in Figure S10, the complexity of our temporal PageRank implementation scales exponentially with the network size.

Multiplex PageRank.

Multiplex PageRank extends PageRank analysis to multiplex networks, in which the same nodes might connect differently across layers. Multiplex PageRank integrates network information from supplementary layers to base layer, as defined by

$$X_{Bi} = \alpha_B \sum_j X_{Ai}{}^{\beta} B_{ij} \frac{X_{Bj}}{G_j} + (1-\alpha_B) \frac{X_{Ai}{}^{\gamma}}{N<X_A{}^{\gamma}>}$$

, where

$$G_j = \sum_r B_{rj} X_{Ar}{}^{\beta} + \delta(0, \sum_r B_{rj} X_{Ar}{}^{\beta})$$

with δ as the Kronecker delta and $< ... >$ as mean value.

In the equation, A and B denote the adjacency matrices of supplementary and base layers. For such adjacency matrices, the first/second subscripts represent the row/column indices. X_{Ai} represent the PageRank value of ith node calculated from B. The same representation rule applies for X_{Bj} and X_{Ar}. N is the total number of nodes in the base layer. α_B is the damping factor used for. β and γ are user-defined parameters. As shown in the equation, multiplex PageRank is calculated according to the topology of the base layer, with regular PageRank of supplemental layer as outgoing weights and personalization vector. For networks with multiple supplementary layers, we can simply multiply their PageRank to fit into the above equation. Based on parameters β and γ, four special multiplex PageRank forms were defined, including additive ($\beta = 0, \gamma = 1$), multiplicative ($\beta = 1, \gamma = 0$), combined ($\beta = 1, \gamma = 1$) and neutral ($\beta = 0, \gamma = 0$) [32]. We implemented the four special forms of multiplex PageRank as the function multiplex_page_rank in R package pageRank, based on CRAN R package igraph [31]. As shown in Figure S10, the complexity of our multiplex PageRank implementation scales exponentially with the network size.

We assume that regulatory machinery can be directly reflected on expression profiles, thus gene expression-based GRNs were used as base networks in this study. In contrast, epigenetic profiles are usually considered as indirect evidence of TF-target regulation. For instance ATAC-Seq and HiChIP GRNs were reverse engineered through motif-matching and TSS-searching, thus significant amounts of false positives should be expected. Also, TFs might not necessarily bind to the regions to be searched, e.g. ATAC-Seq peaks. In the case of ATAC-Seq, TF might bind to enhancer regions, which are usually distant from the corresponding promoters, thus cannot be captured. Therefore, considerable amounts of false negatives should also be expected.

Supplemental References

1. Trapnell, C., Cacchiarelli, D., Grimsby, J., Pokharel, P., Li, S., Morse, M., Lennon, N.J., Livak, K.J., Mikkelsen, T.S. and Rinn, J.L., 2014. The dynamics and regulators of cell fate decisions are revealed by pseudotemporal ordering of single cells. Nature biotechnology, 32(4), p.381.
2. Cao, J., Spielmann, M., Qiu, X., Huang, X., Ibrahim, D.M., Hill, A.J., Zhang, F., Mundlos, S., Christiansen, L., Steemers, F.J. and Trapnell, C., 2019. The single-cell transcriptional landscape of mammalian organogenesis. Nature, 566(7745), pp.496-502.
3. Pliner, H.A., Packer, J.S., McFaline-Figueroa, J.L., Cusanovich, D.A., Daza, R.M., Aghamirzaie, D., Srivatsan, S., Qiu, X., Jackson, D., Minkina, A. and Adey, A.C., 2018. Cicero predicts cis-regulatory DNA interactions from single-cell chromatin accessibility data. Molecular cell, 71(5), pp.858-871.
4. Pellin, D., Loperfido, M., Baricordi, C., Wolock, S.L., Montepeloso, A., Weinberg, O.K., Biffi, A., Klein, A.M. and Biasco, L., 2019. A comprehensive single cell transcriptional landscape of human hematopoietic progenitors. Nature communications, 10(1), pp.1-15.
5. Corces, M.R., Buenrostro, J.D., Wu, B., Greenside, P.G., Chan, S.M., Koenig, J.L., Snyder, M.P., Pritchard, J.K., Kundaje, A., Greenleaf, W.J. and Majeti, R., 2016. Lineage-specific and single-cell chromatin accessibility charts human hematopoiesis and leukemia evolution. Nature genetics, 48(10), pp.1193-1203.
6. Mumbach, M.R., Satpathy, A.T., Boyle, E.A., Dai, C., Gowen, B.G., Cho, S.W., Nguyen, M.L., Rubin, A.J., Granja, J.M., Kazane, K.R. and Wei, Y., 2017. Enhancer connectome in primary human cells identifies target genes of disease-associated DNA elements. Nature genetics, 49(11), p.1602.
7. Alvarez, M.J., Shen, Y., Giorgi, F.M., Lachmann, A., Ding, B.B., Ye, B.H. and Califano, A., 2016. Functional characterization of somatic mutations in cancer using network-based inference of protein activity. Nature genetics, 48(8), pp.838-847.
8. Ding, H., Douglass, E.F., Sonabend, A.M., Mela, A., Bose, S., Gonzalez, C., Canoll, P.D., Sims, P.A., Alvarez, M.J. and Califano, A., 2018. Quantitative assessment of protein activity in orphan tissues and single cells using the metaVIPER algorithm. Nature communications, 9(1), pp.1-10.
9. Aibar, S., González-Blas, C.B., Moerman, T., Imrichova, H., Hulselmans, G., Rambow, F., Marine, J.C., Geurts, P., Aerts, J., van den Oord, J. and Atak, Z.K., 2017. SCENIC: single-cell regulatory network inference and clustering. Nature methods, 14(11), pp.1083-1086.
10. Emmert-Streib, F., Glazko, G. and De Matos Simoes, R., 2012. Statistical inference and reverse engineering of gene regulatory networks from observational expression data. Frontiers in genetics, 3, p.8.
11. Mercatelli, D., Scalambra, L., Triboli, L., Ray, F. and Giorgi, F.M., 2020. Gene regulatory network inference resources: A practical overview. Biochimica et Biophysica Acta (BBA)-Gene Regulatory Mechanisms, 1863(6), p.194430.
12. Basso, K., Margolin, A.A., Stolovitzky, G., Klein, U., Dalla-Favera, R. and Califano, A., 2005. Reverse engineering of regulatory networks in human B cells. Nature genetics, 37(4), pp.382-390.
13. Margolin, A.A., Nemenman, I., Basso, K., Wiggins, C., Stolovitzky, G., Dalla Favera, R. and Califano, A., 2006, March. ARACNE: an algorithm for the reconstruction of gene regulatory networks in a mammalian cellular context. In BMC bioinformatics (Vol. 7, No. S1, p. S7). BioMed Central.
14. Lachmann, A., Giorgi, F.M., Lopez, G. and Califano, A., 2016. ARACNe-AP: gene network reverse engineering through adaptive partitioning inference of mutual information. Bioinformatics, 32(14), pp.2233-2235.
15. Crawford, G.E., Davis, S., Scacheri, P.C., Renaud, G., Halawi, M.J., Erdos, M.R., Green, R., Meltzer, P.S., Wolfsberg, T.G. and Collins, F.S., 2006. DNase-chip: a high-resolution method to identify DNase I hypersensitive sites using tiled microarrays. Nature methods, 3(7), pp.503-509.
16. Sabo, P.J., Kuehn, M.S., Thurman, R., Johnson, B.E., Johnson, E.M., Cao, H., Yu, M., Rosenzweig, E., Goldy, J., Haydock, A. and Weaver, M., 2006. Genome-scale mapping of DNase I sensitivity in vivo using tiling DNA microarrays. Nature methods, 3(7), pp.511-518.

17. Schones, D.E., Cui, K., Cuddapah, S., Roh, T.Y., Barski, A., Wang, Z., Wei, G. and Zhao, K., 2008. Dynamic regulation of nucleosome positioning in the human genome. Cell, 132(5), pp.887-898.
18. Krebs, A.R., Imanci, D., Hoerner, L., Gaidatzis, D., Burger, L. and Schübeler, D., 2017. Genome-wide single-molecule footprinting reveals high RNA polymerase II turnover at paused promoters. Molecular cell, 67(3), pp.411-422.
19. Buenrostro, J.D., Giresi, P.G., Zaba, L.C., Chang, H.Y. and Greenleaf, W.J., 2013. Transposition of native chromatin for fast and sensitive epigenomic profiling of open chromatin, DNA-binding proteins and nucleosome position. Nature methods, 10(12), p.1213.
20. Fullwood, M.J. and Ruan, Y., 2009. ChIP-based methods for the identification of long-range chromatin interactions. Journal of cellular biochemistry, 107(1), pp.30-39.
21. Dekker, J., Rippe, K., Dekker, M. and Kleckner, N., 2002. Capturing chromosome conformation. science, 295(5558), pp.1306-1311.
22. Simonis, M., Klous, P., Splinter, E., Moshkin, Y., Willemsen, R., De Wit, E., Van Steensel, B. and De Laat, W., 2006. Nuclear organization of active and inactive chromatin domains uncovered by chromosome conformation capture–on-chip (4C). Nature genetics, 38(11), pp.1348-1354.
23. Dostie, J., Richmond, T.A., Arnaout, R.A., Selzer, R.R., Lee, W.L., Honan, T.A., Rubio, E.D., Krumm, A., Lamb, J., Nusbaum, C. and Green, R.D., 2006. Chromosome Conformation Capture Carbon Copy (5C): a massively parallel solution for mapping interactions between genomic elements. Genome research, 16(10), pp.1299-1309.
24. Lieberman-Aiden, E., Van Berkum, N.L., Williams, L., Imakaev, M., Ragoczy, T., Telling, A., Amit, I., Lajoie, B.R., Sabo, P.J., Dorschner, M.O. and Sandstrom, R., 2009. Comprehensive mapping of long-range interactions reveals folding principles of the human genome. science, 326(5950), pp.289-293.
25. Carlson, M.R., Pagès, H., Arora, S., Obenchain, V. and Morgan, M., 2016. Genomic annotation resources in R/Bioconductor. In Statistical Genomics (pp. 67-90). Humana Press, New York, NY.
26. Lawrence, M., Huber, W., Pages, H., Aboyoun, P., Carlson, M., Gentleman, R., Morgan, M.T. and Carey, V.J., 2013. Software for computing and annotating genomic ranges. PLoS Comput Biol, 9(8), p.e1003118.
27. Khan, A., Fornes, O., Stigliani, A., Gheorghe, M., Castro-Mondragon, J.A., Van Der Lee, R., Bessy, A., Chèneby, J., Kulkarni, S.R., Tan, G. and Baranasic, D., 2018. JASPAR 2018: update of the open-access database of transcription factor binding profiles and its web framework. Nucleic acids research, 46(D1), pp.D260-D266.
28. Tan, G. and Lenhard, B., 2016. TFBSTools: an R/bioconductor package for transcription factor binding site analysis. Bioinformatics, 32(10), pp.1555-1556.
29. Schep, A.N., Wu, B., Buenrostro, J.D. and Greenleaf, W.J., 2017. chromVAR: inferring transcription-factor-associated accessibility from single-cell epigenomic data. Nature methods, 14(10), pp.975-978.
30. Rozenshtein, P. and Gionis, A., 2016, September. Temporal pagerank. In Joint European Conference on Machine Learning and Knowledge Discovery in Databases (pp. 674-689). Springer, Cham.
31. Csardi, G. and Nepusz, T., 2006. The igraph software package for complex network research. InterJournal, complex systems, 1695(5), pp.1-9.
32. Halu, A., Mondragón, R.J., Panzarasa, P. and Bianconi, G., 2013. Multiplex pagerank. PloS one, 8(10), p.e78293.

scRNA−Seq T0

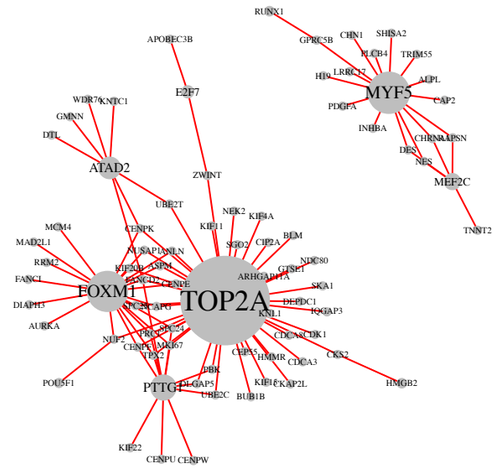

scRNA−Seq T24

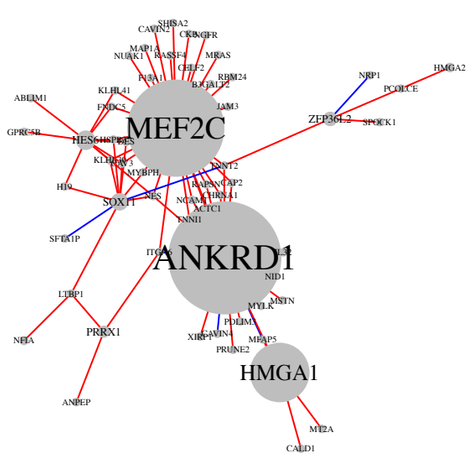

scRNA−Seq T48

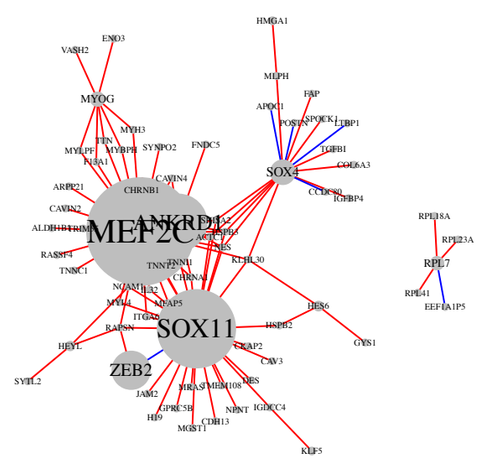

scRNA−Seq T72

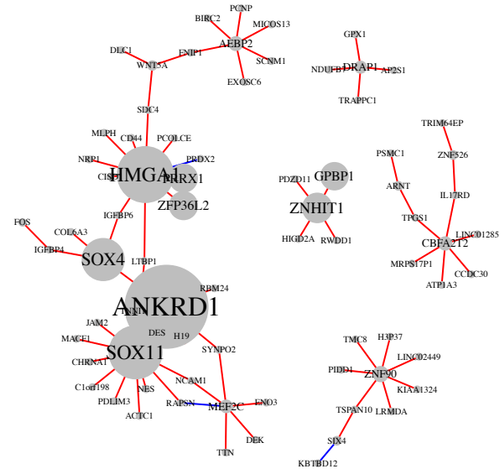

ATAC−Seq T0

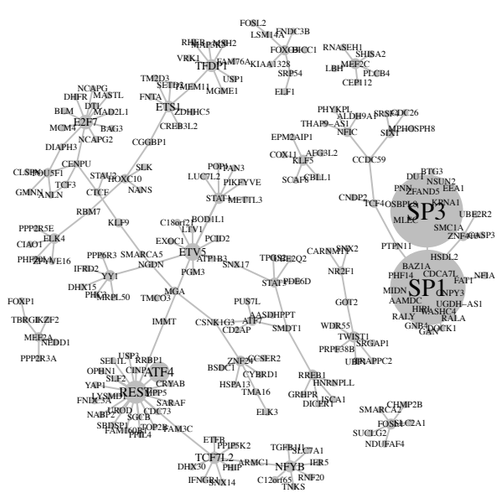

ATAC−Seq T24

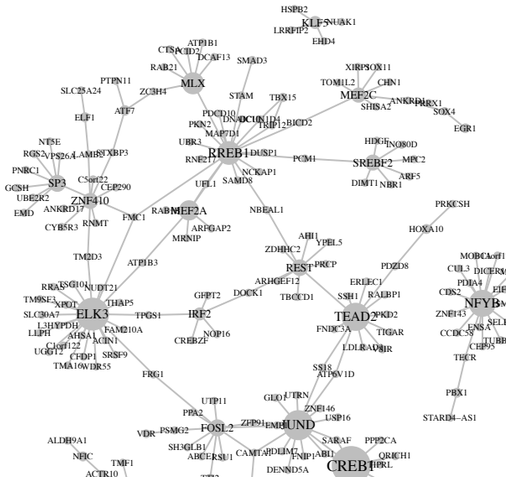

ATAC−Seq T48

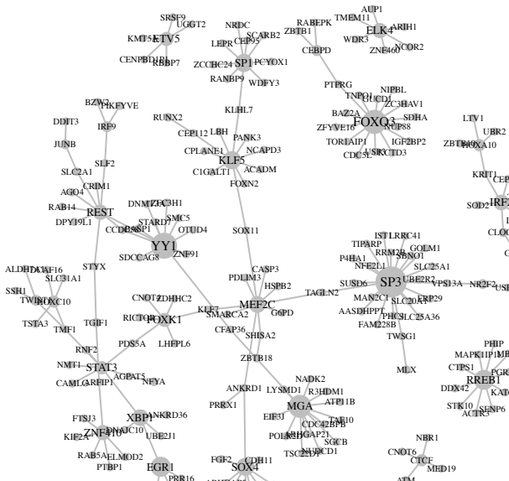

ATAC−Seq T72

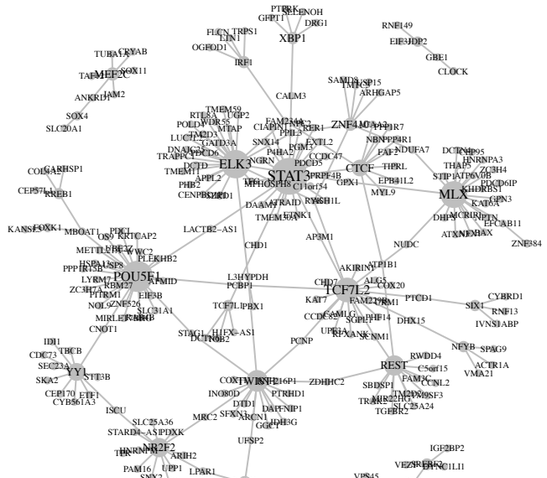

scRNA−Seq T0−>T24

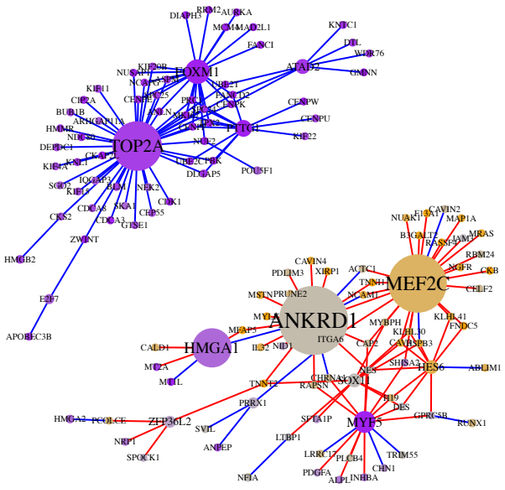

scRNA−Seq T24−>T48

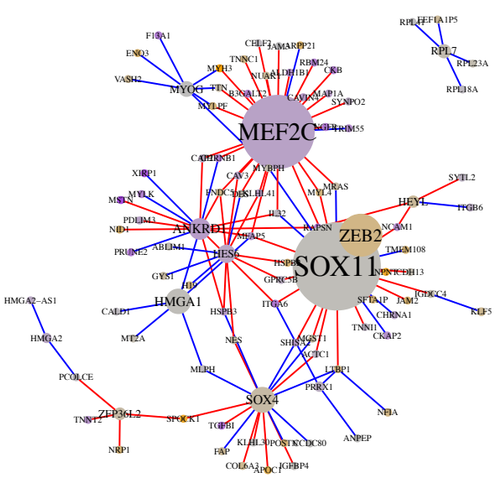

scRNA−Seq T48−>T72

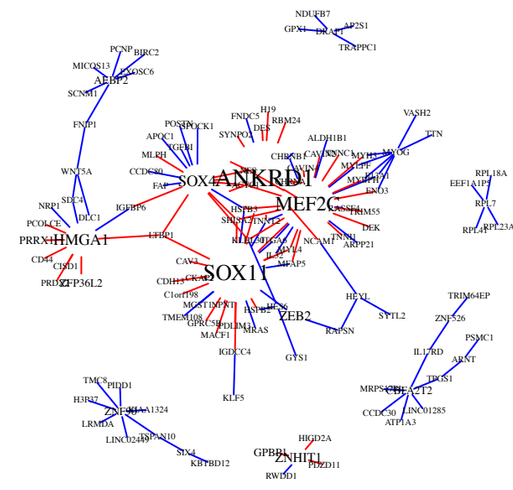

ATAC−Seq T0−>T24

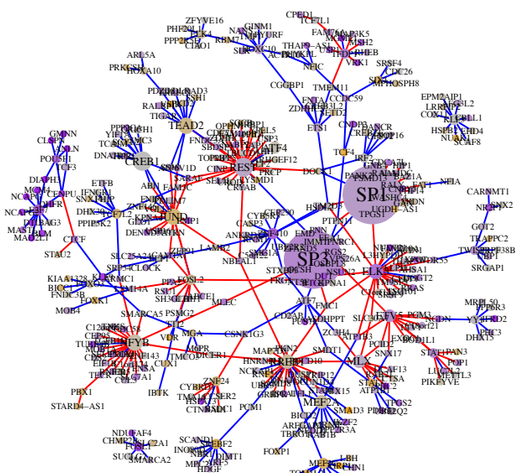

ATAC−Seq T24−>T48

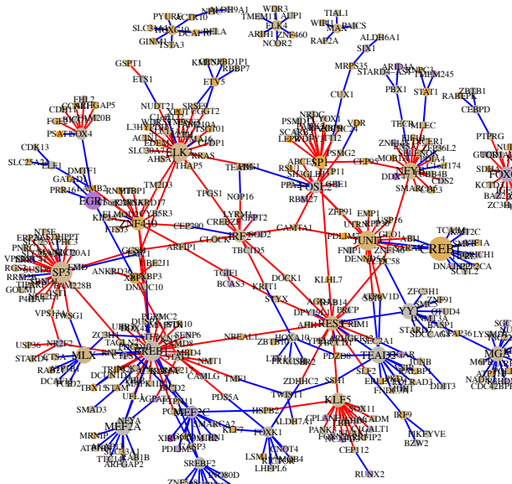

ATAC−Seq T48−>T72

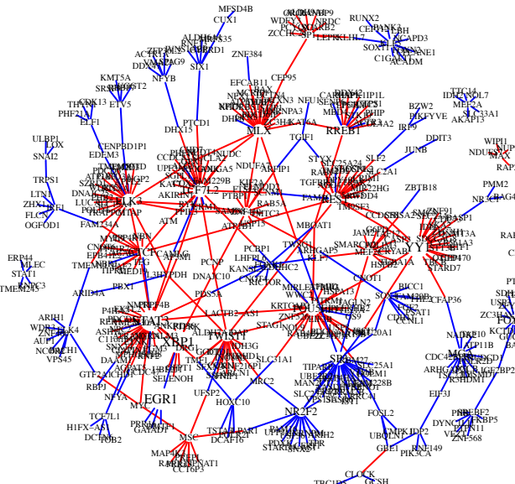

Figure S1

Chondrocyte–progenitors

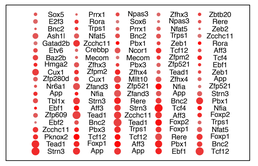

Chondrocytes–&–osteoblasts

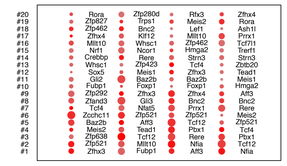

Connective–tissue–progenitors

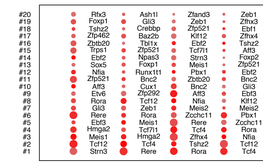

Definitive–erythroid–lineage

Early–mesenchyme

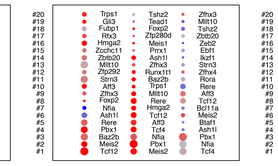

Endothelial–cells

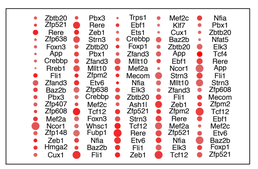

Ependymal–cell

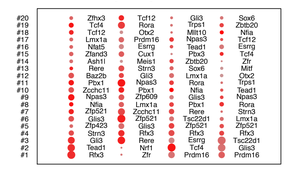

Epithelial–cells

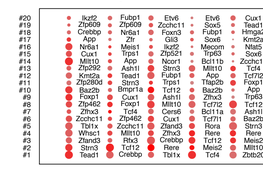

Excitatory–neurons

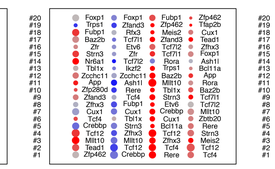

Granule–neurons

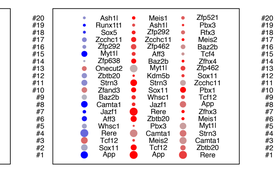

Hepatocytes

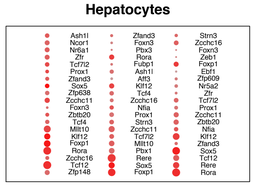

Inhibitory–interneurons

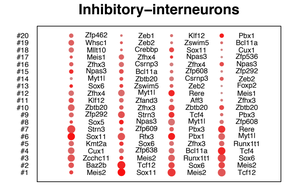

Inhibitory–neuron–progenitors

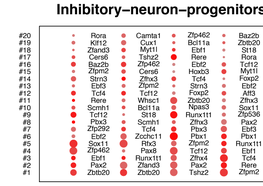

Inhibitory–neurons

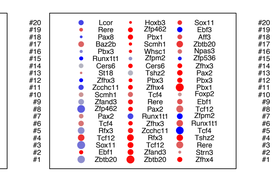

Intermediate–Mesoderm

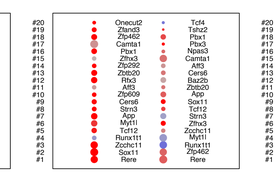

Isthmic–organizer–cells

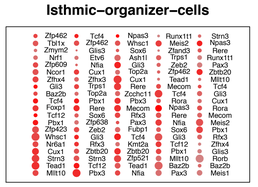

Jaw–and–tooth–progenitors

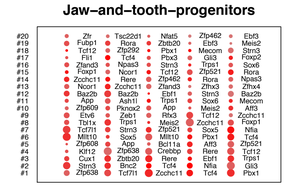

Limb–mesenchyme

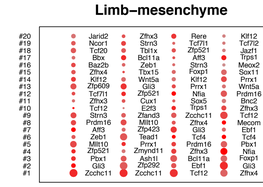

Megakaryocytes

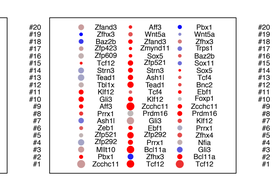

Myocytes

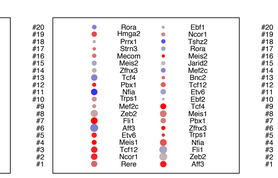

Neural–progenitor–cells

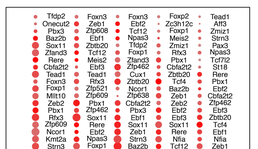

Neural–Tube

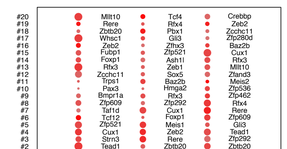

Notochord–cells

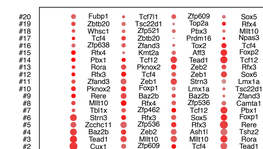

Oligodendrocyte–Progenitors

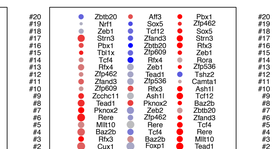

Osteoblasts

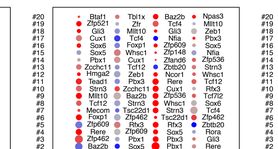

Postmitotic–premature–neurons

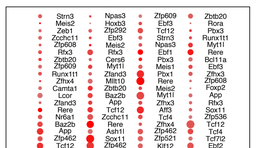

Premature–oligodendrocyte

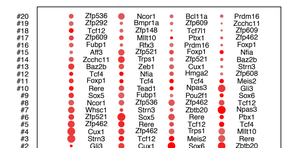

Primitive–erythroid–lineage

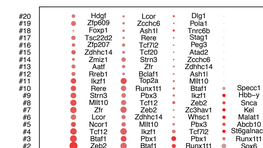

Radial–glia

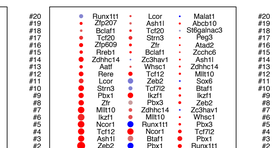

Schwann–cell–precursor

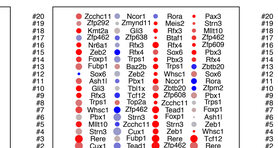

Sensory–neurons

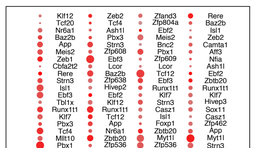

Stromal–cells

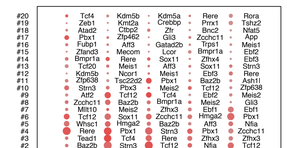

White–blood–cells

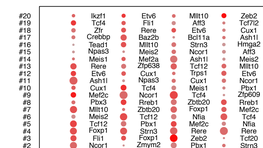

Figure S2

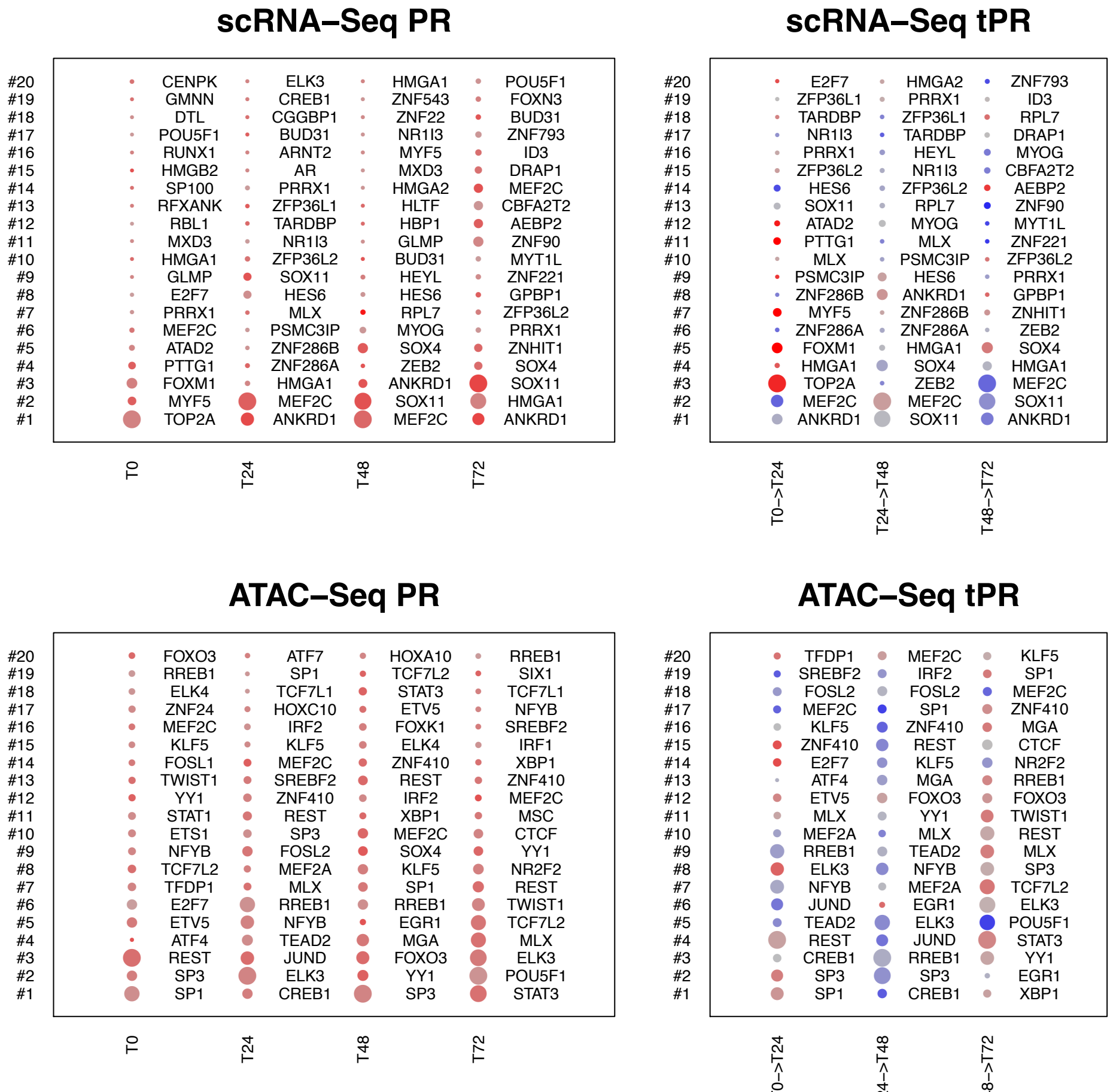
scRNA–Seq PR
#20 CENPK ELK3 HMGA1 POU5F1
#19 GMNN CREB1 ZNF543 FOXN3
#18 DTL CGGBP1 ZNF22 BUD31
#17 POU5F1 BUD31 NR1I3 ZNF793
#16 RUNX1 ARNT2 MYF5 ID3
#15 HMGB2 AR MXD3 DRAP1
#14 SP100 PRRX1 HMGA2 MEF2C
#13 RFXANK ZFP36L1 HLTF CBFA2T2
#12 RBL1 TARDBP HBP1 AEBP2
#11 MXD3 NR1I3 GLMP ZNF90
#10 HMGA1 ZFP36L2 BUD31 MYT1L
#9 GLMP SOX11 HEYL ZNF221
#8 E2F7 HES6 HES6 GPBP1
#7 PRRX1 MLX RPL7 ZFP36L2
#6 MEF2C PSMC3IP MYOG PRRX1
#5 ATAD2 ZNF286B SOX4 ZNHIT1
#4 PTTG1 ZNF286A ZEB2 SOX4
#3 FOXM1 HMGA1 ANKRD1 SOX11
#2 MYF5 MEF2C SOX11 HMGA1
#1 TOP2A ANKRD1 MEF2C ANKRD1
T0
T24
T48
T72
scRNA–Seq tPR
#20 E2F7 HMGA2 ZNF793
#19 ZFP36L1 PRRX1 ID3
#18 TARDBP ZFP36L1 RPL7
#17 NR1I3 TARDBP DRAP1
#16 PRRX1 HEYL MYOG
#15 ZFP36L2 NR1I3 CBFA2T2
#14 HES6 ZFP36L2 AEBP2
#13 SOX11 RPL7 ZNF90
#12 ATAD2 MYOG MYT1L
#11 PTTG1 MLX ZNF221
#10 MLX PSMC3IP ZFP36L2
#9 PSMC3IP HES6 PRRX1
#8 ZNF286B ANKRD1 GPBP1
#7 MYF5 ZNF286B ZNHIT1
#6 ZNF286A ZNF286A ZEB2
#5 FOXM1 HMGA1 SOX4
#4 HMGA1 SOX4 HMGA1
#3 TOP2A ZEB2 MEF2C
#2 MEF2C MEF2C SOX11
#1 ANKRD1 SOX11 ANKRD1
T0–>T24
T24–>T48
T48–>T72
ATAC–Seq PR
#20 FOXO3 ATF7 HOXA10 RREB1
#19 RREB1 SP1 TCF7L2 SIX1
#18 ELK4 TCF7L1 STAT3 TCF7L1
#17 ZNF24 HOXC10 ETV5 NFYB
#16 MEF2C IRF2 FOXK1 SREBF2
#15 KLF5 KLF5 ELK4 IRF1
#14 FOSL1 MEF2C ZNF410 XBP1
#13 TWIST1 SREBF2 REST ZNF410
#12 YY1 ZNF410 IRF2 MEF2C
#11 STAT1 REST XBP1 MSC
#10 ETS1 SP3 MEF2C CTCF
#9 NFYB FOSL2 SOX4 YY1
#8 TCF7L2 MEF2A KLF5 NR2F2
#7 TFDP1 MLX SP1 REST
#6 E2F7 RREB1 RREB1 TWIST1
#5 ETV5 NFYB EGR1 TCF7L2
#4 ATF4 TEAD2 MGA MLX
#3 REST JUND FOXO3 ELK3
#2 SP3 ELK3 YY1 POU5F1
#1 SP1 CREB1 SP3 STAT3
T0
T24
T48
T72
ATAC–Seq tPR
#20 TFDP1 MEF2C KLF5
#19 SREBF2 IRF2 SP1
#18 FOSL2 FOSL2 MEF2C
#17 MEF2C SP1 ZNF410
#16 KLF5 ZNF410 MGA
#15 ZNF410 REST CTCF
#14 E2F7 KLF5 NR2F2
#13 ATF4 MGA RREB1
#12 ETV5 FOXO3 FOXO3
#11 MLX YY1 TWIST1
#10 MEF2A MLX REST
#9 RREB1 TEAD2 MLX
#8 ELK3 NFYB SP3
#7 NFYB MEF2A TCF7L2
#6 JUND EGR1 ELK3
#5 TEAD2 ELK3 POU5F1
#4 REST JUND STAT3
#3 CREB1 RREB1 YY1
#2 SP3 SP3 EGR1
#1 SP1 CREB1 XBP1
T0–>T24
T24–>T48
T48–>T72

Figure S3

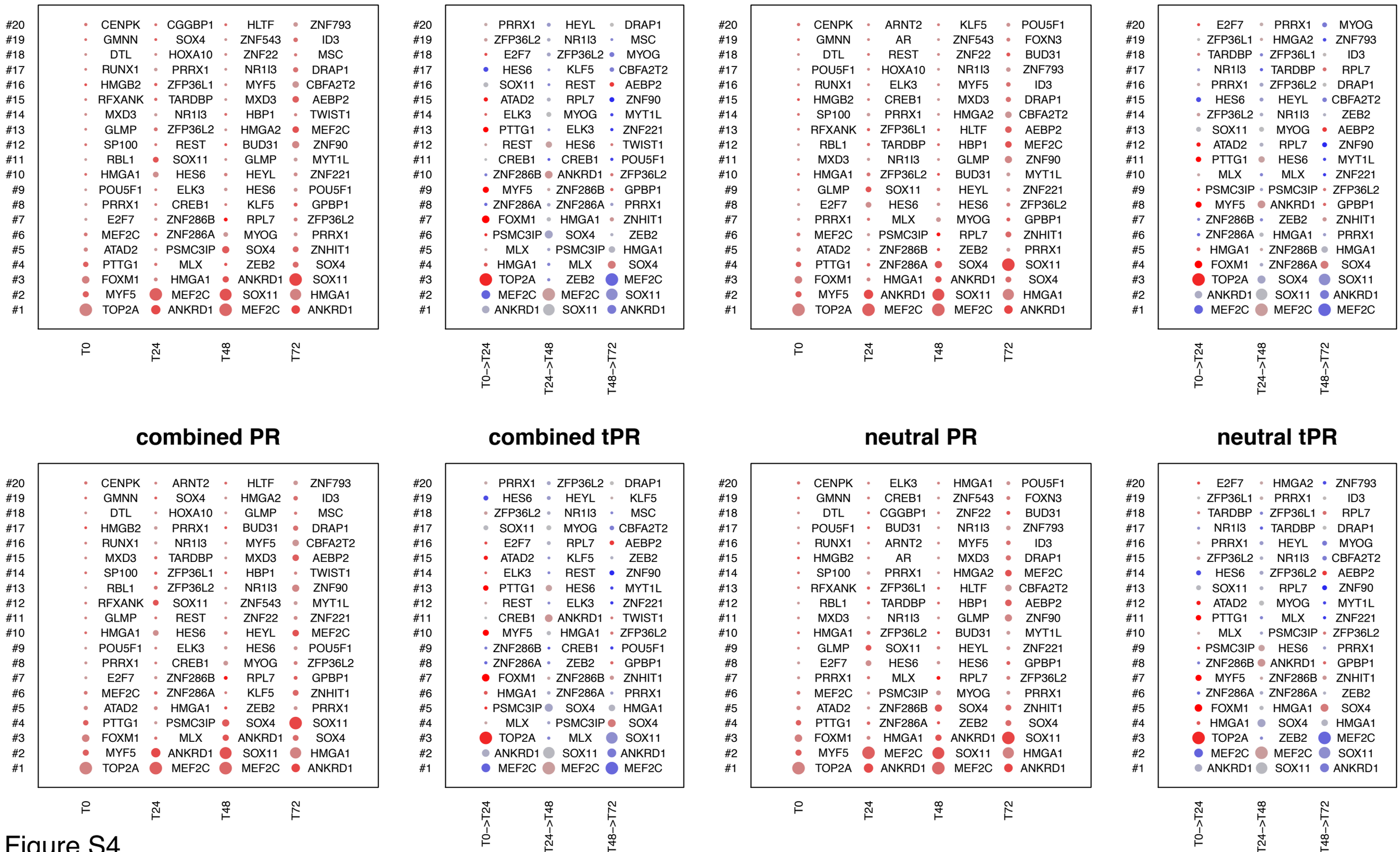
additive PR
#20 CENPK CGGBP1 HLTF ZNF793
#19 GMNN SOX4 ZNF543 ID3
#18 DTL HOXA10 ZNF22 MSC
#17 RUNX1 PRRX1 NR1I3 DRAP1
#16 HMGB2 ZFP36L1 MYF5 CBFA2T2
#15 RFXANK TARDBP MXD3 AEBP2
#14 MXD3 NR1I3 HBP1 TWIST1
#13 GLMP ZFP36L2 HMGA2 MEF2C
#12 SP100 REST BUD31 ZNF90
#11 RBL1 SOX11 GLMP MYT1L
#10 HMGA1 HES6 HEYL ZNF221
#9 POU5F1 ELK3 HES6 POU5F1
#8 PRRX1 CREB1 KLF5 GPBP1
#7 E2F7 ZNF286B RPL7 ZFP36L2
#6 MEF2C ZNF286A MYOG PRRX1
#5 ATAD2 PSMC3IP SOX4 ZNHIT1
#4 PTTG1 MLX ZEB2 SOX4
#3 FOXM1 HMGA1 ANKRD1 SOX11
#2 MYF5 MEF2C SOX11 HMGA1
#1 TOP2A ANKRD1 MEF2C ANKRD1
T0
T24
T48
T72
additive tPR
#20 PRRX1 HEYL DRAP1
#19 ZFP36L2 NR1I3 MSC
#18 E2F7 ZFP36L2 MYOG
#17 HES6 KLF5 CBFA2T2
#16 SOX11 REST AEBP2
#15 ATAD2 RPL7 ZNF90
#14 ELK3 MYOG MYT1L
#13 PTTG1 ELK3 ZNF221
#12 REST HES6 TWIST1
#11 CREB1 CREB1 POU5F1
#10 ZNF286B ANKRD1 ZFP36L2
#9 MYF5 ZNF286B GPBP1
#8 ZNF286A ZNF286A PRRX1
#7 FOXM1 HMGA1 ZNHIT1
#6 PSMC3IP SOX4 ZEB2
#5 MLX PSMC3IP HMGA1
#4 HMGA1 MLX SOX4
#3 TOP2A ZEB2 MEF2C
#2 MEF2C MEF2C SOX11
#1 ANKRD1 SOX11 ANKRD1
T0->T24
T24->T48
T48->T72
multiplicative PR
#20 CENPK ARNT2 KLF5 POU5F1
#19 GMNN AR ZNF543 FOXN3
#18 DTL REST ZNF22 BUD31
#17 POU5F1 HOXA10 NR1I3 ZNF793
#16 RUNX1 ELK3 MYF5 ID3
#15 HMGB2 CREB1 MXD3 DRAP1
#14 SP100 PRRX1 HMGA2 CBFA2T2
#13 RFXANK ZFP36L1 HLTF AEBP2
#12 RBL1 TARDBP HBP1 MEF2C
#11 MXD3 NR1I3 GLMP ZNF90
#10 HMGA1 ZFP36L2 BUD31 MYT1L
#9 GLMP SOX11 HEYL ZNF221
#8 E2F7 HES6 HES6 ZFP36L2
#7 PRRX1 MLX MYOG GPBP1
#6 MEF2C PSMC3IP RPL7 ZNHIT1
#5 ATAD2 ZNF286B ZEB2 PRRX1
#4 PTTG1 ZNF286A SOX4 SOX11
#3 FOXM1 HMGA1 ANKRD1 SOX4
#2 MYF5 ANKRD1 SOX11 HMGA1
#1 TOP2A MEF2C MEF2C ANKRD1
T0
T24
T48
T72
multiplicative tPR
#20 E2F7 PRRX1 MYOG
#19 ZFP36L1 HMGA2 ZNF793
#18 TARDBP ZFP36L1 ID3
#17 NR1I3 TARDBP RPL7
#16 PRRX1 ZFP36L2 DRAP1
#15 HES6 HEYL CBFA2T2
#14 ZFP36L2 NR1I3 ZEB2
#13 SOX11 MYOG AEBP2
#12 ATAD2 RPL7 ZNF90
#11 PTTG1 HES6 MYT1L
#10 MLX MLX ZNF221
#9 PSMC3IP PSMC3IP ZFP36L2
#8 MYF5 ANKRD1 GPBP1
#7 ZNF286B ZEB2 ZNHIT1
#6 ZNF286A HMGA1 PRRX1
#5 HMGA1 ZNF286B HMGA1
#4 FOXM1 ZNF286A SOX4
#3 TOP2A SOX4 SOX11
#2 ANKRD1 SOX11 ANKRD1
#1 MEF2C MEF2C MEF2C
T0->T24
T24->T48
T48->T72
combined PR
#20 CENPK ARNT2 HLTF ZNF793
#19 GMNN SOX4 HMGA2 ID3
#18 DTL HOXA10 GLMP MSC
#17 HMGB2 PRRX1 BUD31 DRAP1
#16 RUNX1 NR1I3 MYF5 CBFA2T2
#15 MXD3 TARDBP MXD3 AEBP2
#14 SP100 ZFP36L1 HBP1 TWIST1
#13 RBL1 ZFP36L2 NR1I3 ZNF90
#12 RFXANK SOX11 ZNF543 MYT1L
#11 GLMP REST ZNF22 ZNF221
#10 HMGA1 HES6 HEYL MEF2C
#9 POU5F1 ELK3 HES6 POU5F1
#8 PRRX1 CREB1 MYOG ZFP36L2
#7 E2F7 ZNF286B RPL7 GPBP1
#6 MEF2C ZNF286A KLF5 ZNHIT1
#5 ATAD2 HMGA1 ZEB2 PRRX1
#4 PTTG1 PSMC3IP SOX4 SOX11
#3 FOXM1 MLX ANKRD1 SOX4
#2 MYF5 ANKRD1 SOX11 HMGA1
#1 TOP2A MEF2C MEF2C ANKRD1
T0
T24
T48
T72
combined tPR
#20 PRRX1 ZFP36L2 DRAP1
#19 HES6 HEYL KLF5
#18 ZFP36L2 NR1I3 MSC
#17 SOX11 MYOG CBFA2T2
#16 E2F7 RPL7 AEBP2
#15 ATAD2 KLF5 ZEB2
#14 ELK3 REST ZNF90
#13 PTTG1 HES6 MYT1L
#12 REST ELK3 ZNF221
#11 CREB1 ANKRD1 TWIST1
#10 MYF5 HMGA1 ZFP36L2
#9 ZNF286B CREB1 POU5F1
#8 ZNF286A ZEB2 GPBP1
#7 FOXM1 ZNF286B ZNHIT1
#6 HMGA1 ZNF286A PRRX1
#5 PSMC3IP SOX4 HMGA1
#4 MLX PSMC3IP SOX4
#3 TOP2A MLX SOX11
#2 ANKRD1 SOX11 ANKRD1
#1 MEF2C MEF2C MEF2C
T0->T24
T24->T48
T48->T72
neutral PR
#20 CENPK ELK3 HMGA1 POU5F1
#19 GMNN CREB1 ZNF543 FOXN3
#18 DTL CGGBP1 ZNF22 BUD31
#17 POU5F1 BUD31 NR1I3 ZNF793
#16 RUNX1 ARNT2 MYF5 ID3
#15 HMGB2 AR MXD3 DRAP1
#14 SP100 PRRX1 HMGA2 MEF2C
#13 RFXANK ZFP36L1 HLTF CBFA2T2
#12 RBL1 TARDBP HBP1 AEBP2
#11 MXD3 NR1I3 GLMP ZNF90
#10 HMGA1 ZFP36L2 BUD31 MYT1L
#9 GLMP SOX11 HEYL ZNF221
#8 E2F7 HES6 HES6 GPBP1
#7 PRRX1 MLX RPL7 ZFP36L2
#6 MEF2C PSMC3IP MYOG PRRX1
#5 ATAD2 ZNF286B SOX4 ZNHIT1
#4 PTTG1 ZNF286A ZEB2 SOX4
#3 FOXM1 HMGA1 ANKRD1 SOX11
#2 MYF5 MEF2C SOX11 HMGA1
#1 TOP2A ANKRD1 MEF2C ANKRD1
T0
T24
T48
T72
neutral tPR
#20 E2F7 HMGA2 ZNF793
#19 ZFP36L1 PRRX1 ID3
#18 TARDBP ZFP36L1 RPL7
#17 NR1I3 TARDBP DRAP1
#16 PRRX1 HEYL MYOG
#15 ZFP36L2 NR1I3 CBFA2T2
#14 HES6 ZFP36L2 AEBP2
#13 SOX11 RPL7 ZNF90
#12 ATAD2 MYOG MYT1L
#11 PTTG1 MLX ZNF221
#10 MLX PSMC3IP ZFP36L2
#9 PSMC3IP HES6 PRRX1
#8 ZNF286B ANKRD1 GPBP1
#7 MYF5 ZNF286B ZNHIT1
#6 ZNF286A ZNF286A ZEB2
#5 FOXM1 HMGA1 HMGA1
#4 HMGA1 SOX4 SOX4
#3 TOP2A ZEB2 MEF2C
#2 MEF2C MEF2C SOX11
#1 ANKRD1 SOX11 ANKRD1
T0->T24
T24->T48
T48->T72

Figure S4

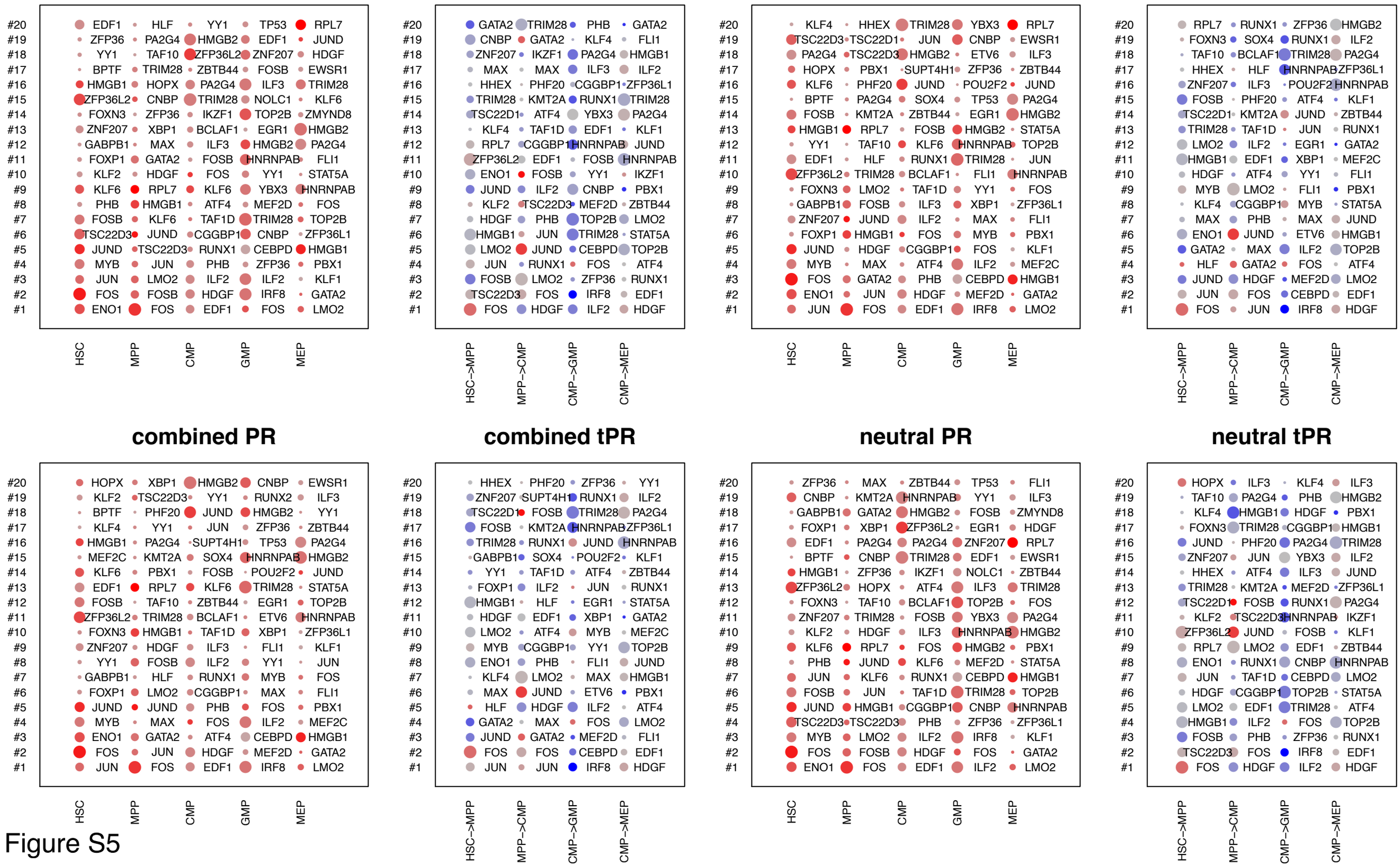
additive PR
#20 EDF1 HLF YY1 TP53 RPL7
#19 ZFP36 PA2G4 HMGB2 EDF1 JUND
#18 YY1 TAF10 ZFP36L2 ZNF207 HDGF
#17 BPTF TRIM28 ZBTB44 FOSB EWSR1
#16 HMGB1 HOPX PA2G4 ILF3 TRIM28
#15 ZFP36L2 CNBP TRIM28 NOLC1 KLF6
#14 FOXN3 ZFP36 IKZF1 TOP2B ZMYND8
#13 ZNF207 XBP1 BCLAF1 EGR1 HMGB2
#12 GABPB1 MAX ILF3 HMGB2 PA2G4
#11 FOXP1 GATA2 FOSB HNRNPAB FLI1
#10 KLF2 HDGF FOS YY1 STAT5A
#9 KLF6 RPL7 KLF6 YBX3 HNRNPAB
#8 PHB HMGB1 ATF4 MEF2D FOS
#7 FOSB KLF6 TAF1D TRIM28 TOP2B
#6 TSC22D3 JUND CGGBP1 CNBP ZFP36L1
#5 JUND TSC22D3 RUNX1 CEBPD HMGB1
#4 MYB JUN PHB ZFP36 PBX1
#3 JUN LMO2 ILF2 ILF2 KLF1
#2 FOS FOSB HDGF IRF8 GATA2
#1 ENO1 FOS EDF1 FOS LMO2
HSC MPP CMP GMP MEP
additive tPR
#20 GATA2 TRIM28 PHB GATA2
#19 CNBP GATA2 KLF4 FLI1
#18 ZNF207 IKZF1 PA2G4 HMGB1
#17 MAX MAX ILF3 ILF2
#16 HHEX PHF20 CGGBP1 ZFP36L1
#15 TRIM28 KMT2A RUNX1 TRIM28
#14 TSC22D1 ATF4 YBX3 PA2G4
#13 KLF4 TAF1D EDF1 KLF1
#12 RPL7 CGGBP1 HNRNPAB JUND
#11 ZFP36L2 EDF1 FOSB HNRNPAB
#10 ENO1 FOSB YY1 IKZF1
#9 JUND ILF2 CNBP PBX1
#8 KLF2 TSC22D3 MEF2D ZBTB44
#7 HDGF PHB TOP2B LMO2
#6 HMGB1 JUN TRIM28 STAT5A
#5 LMO2 JUND CEBPD TOP2B
#4 JUN RUNX1 FOS ATF4
#3 FOSB LMO2 ZFP36 RUNX1
#2 TSC22D3 FOS IRF8 EDF1
#1 FOS HDGF ILF2 HDGF
HSC->MPP MPP->CMP CMP->GMP CMP->MEP
multiplicative PR
#20 KLF4 HHEX TRIM28 YBX3 RPL7
#19 TSC22D3 TSC22D1 JUN CNBP EWSR1
#18 PA2G4 TSC22D3 HMGB2 ETV6 ILF3
#17 HOPX PBX1 SUPT4H1 ZFP36 ZBTB44
#16 KLF6 PHF20 JUND POU2F2 JUND
#15 BPTF PA2G4 SOX4 TP53 PA2G4
#14 FOSB KMT2A ZBTB44 EGR1 HMGB2
#13 HMGB1 RPL7 FOSB HMGB2 STAT5A
#12 YY1 TAF10 KLF6 HNRNPAB TOP2B
#11 EDF1 HLF RUNX1 TRIM28 JUN
#10 ZFP36L2 TRIM28 BCLAF1 FLI1 HNRNPAB
#9 FOXN3 LMO2 TAF1D YY1 FOS
#8 GABPB1 FOSB ILF3 XBP1 ZFP36L1
#7 ZNF207 JUND ILF2 MAX FLI1
#6 FOXP1 HMGB1 FOS MYB PBX1
#5 JUND HDGF CGGBP1 FOS KLF1
#4 MYB MAX ATF4 ILF2 MEF2C
#3 FOS GATA2 PHB CEBPD HMGB1
#2 ENO1 JUN HDGF MEF2D GATA2
#1 JUN FOS EDF1 IRF8 LMO2
HSC MPP CMP GMP MEP
multiplicative tPR
#20 RPL7 RUNX1 ZFP36 HMGB2
#19 FOXN3 SOX4 RUNX1 ILF2
#18 TAF10 BCLAF1 TRIM28 PA2G4
#17 HHEX HLF HNRNPAB ZFP36L1
#16 ZNF207 ILF3 POU2F2 HNRNPAB
#15 FOSB PHF20 ATF4 KLF1
#14 TSC22D1 KMT2A JUND ZBTB44
#13 TRIM28 TAF1D JUN RUNX1
#12 LMO2 ILF2 EGR1 GATA2
#11 HMGB1 EDF1 XBP1 MEF2C
#10 HDGF ATF4 YY1 FLI1
#9 MYB LMO2 FLI1 PBX1
#8 KLF4 CGGBP1 MYB STAT5A
#7 MAX PHB MAX JUND
#6 ENO1 JUND ETV6 HMGB1
#5 GATA2 MAX ILF2 TOP2B
#4 HLF GATA2 FOS ATF4
#3 JUND HDGF MEF2D LMO2
#2 JUN FOS CEBPD EDF1
#1 FOS JUN IRF8 HDGF
HSC->MPP MPP->CMP CMP->GMP CMP->MEP
combined PR
#20 HOPX XBP1 HMGB2 CNBP EWSR1
#19 KLF2 TSC22D3 YY1 RUNX2 ILF3
#18 BPTF PHF20 JUND HMGB2 YY1
#17 KLF4 YY1 JUN ZFP36 ZBTB44
#16 HMGB1 PA2G4 SUPT4H1 TP53 PA2G4
#15 MEF2C KMT2A SOX4 HNRNPAB HMGB2
#14 KLF6 PBX1 FOSB POU2F2 JUND
#13 EDF1 RPL7 KLF6 TRIM28 STAT5A
#12 FOSB TAF10 ZBTB44 EGR1 TOP2B
#11 ZFP36L2 TRIM28 BCLAF1 ETV6 HNRNPAB
#10 FOXN3 HMGB1 TAF1D XBP1 ZFP36L1
#9 ZNF207 HDGF ILF3 FLI1 KLF1
#8 YY1 FOSB ILF2 YY1 JUN
#7 GABPB1 HLF RUNX1 MYB FOS
#6 FOXP1 LMO2 CGGBP1 MAX FLI1
#5 JUND JUND PHB FOS PBX1
#4 MYB MAX FOS ILF2 MEF2C
#3 ENO1 GATA2 ATF4 CEBPD HMGB1
#2 FOS JUN HDGF MEF2D GATA2
#1 JUN FOS EDF1 IRF8 LMO2
HSC MPP CMP GMP MEP
combined tPR
#20 HHEX PHF20 ZFP36 YY1
#19 ZNF207 SUPT4H1 RUNX1 ILF2
#18 TSC22D1 FOSB TRIM28 PA2G4
#17 FOSB KMT2A HNRNPAB ZFP36L1
#16 TRIM28 RUNX1 JUND HNRNPAB
#15 GABPB1 SOX4 POU2F2 KLF1
#14 YY1 TAF1D ATF4 ZBTB44
#13 FOXP1 ILF2 JUN RUNX1
#12 HMGB1 HLF EGR1 STAT5A
#11 HDGF EDF1 XBP1 GATA2
#10 LMO2 ATF4 MYB MEF2C
#9 MYB CGGBP1 YY1 TOP2B
#8 ENO1 PHB FLI1 JUND
#7 KLF4 LMO2 MAX HMGB1
#6 MAX JUND ETV6 PBX1
#5 HLF HDGF ILF2 ATF4
#4 GATA2 MAX FOS LMO2
#3 JUND GATA2 MEF2D FLI1
#2 FOS FOS CEBPD EDF1
#1 JUN JUN IRF8 HDGF
HSC->MPP MPP->CMP CMP->GMP CMP->MEP
neutral PR
#20 ZFP36 MAX ZBTB44 TP53 FLI1
#19 CNBP KMT2A HNRNPAB YY1 ILF3
#18 GABPB1 GATA2 HMGB2 FOSB ZMYND8
#17 FOXP1 XBP1 ZFP36L2 EGR1 HDGF
#16 EDF1 PA2G4 PA2G4 ZNF207 RPL7
#15 BPTF CNBP TRIM28 EDF1 EWSR1
#14 HMGB1 ZFP36 IKZF1 NOLC1 ZBTB44
#13 ZFP36L2 HOPX ATF4 ILF3 TRIM28
#12 FOXN3 TAF10 BCLAF1 TOP2B FOS
#11 ZNF207 TRIM28 FOSB YBX3 PA2G4
#10 KLF2 HDGF ILF3 HNRNPAB HMGB2
#9 KLF6 RPL7 FOS HMGB2 PBX1
#8 PHB JUND KLF6 MEF2D STAT5A
#7 JUN KLF6 RUNX1 CEBPD HMGB1
#6 FOSB JUN TAF1D TRIM28 TOP2B
#5 JUND HMGB1 CGGBP1 CNBP HNRNPAB
#4 TSC22D3 TSC22D3 PHB ZFP36 ZFP36L1
#3 MYB LMO2 ILF2 IRF8 KLF1
#2 FOS FOSB HDGF FOS GATA2
#1 ENO1 FOS EDF1 ILF2 LMO2
HSC MPP CMP GMP MEP
neutral tPR
#20 HOPX ILF3 KLF4 ILF3
#19 TAF10 PA2G4 PHB HMGB2
#18 KLF4 HMGB1 HDGF PBX1
#17 FOXN3 TRIM28 CGGBP1 HMGB1
#16 JUND PHF20 PA2G4 TRIM28
#15 ZNF207 JUN YBX3 ILF2
#14 HHEX ATF4 ILF3 JUND
#13 TRIM28 KMT2A MEF2D ZFP36L1
#12 TSC22D1 FOSB RUNX1 PA2G4
#11 KLF2 TSC22D3 HNRNPAB IKZF1
#10 ZFP36L2 JUND FOSB KLF1
#9 RPL7 LMO2 EDF1 ZBTB44
#8 ENO1 RUNX1 CNBP HNRNPAB
#7 JUN TAF1D CEBPD LMO2
#6 HDGF CGGBP1 TOP2B STAT5A
#5 LMO2 EDF1 TRIM28 ATF4
#4 HMGB1 ILF2 FOS TOP2B
#3 FOSB PHB ZFP36 RUNX1
#2 TSC22D3 FOS IRF8 EDF1
#1 FOS HDGF ILF2 HDGF
HSC->MPP MPP->CMP CMP->GMP CMP->MEP

Figure S5

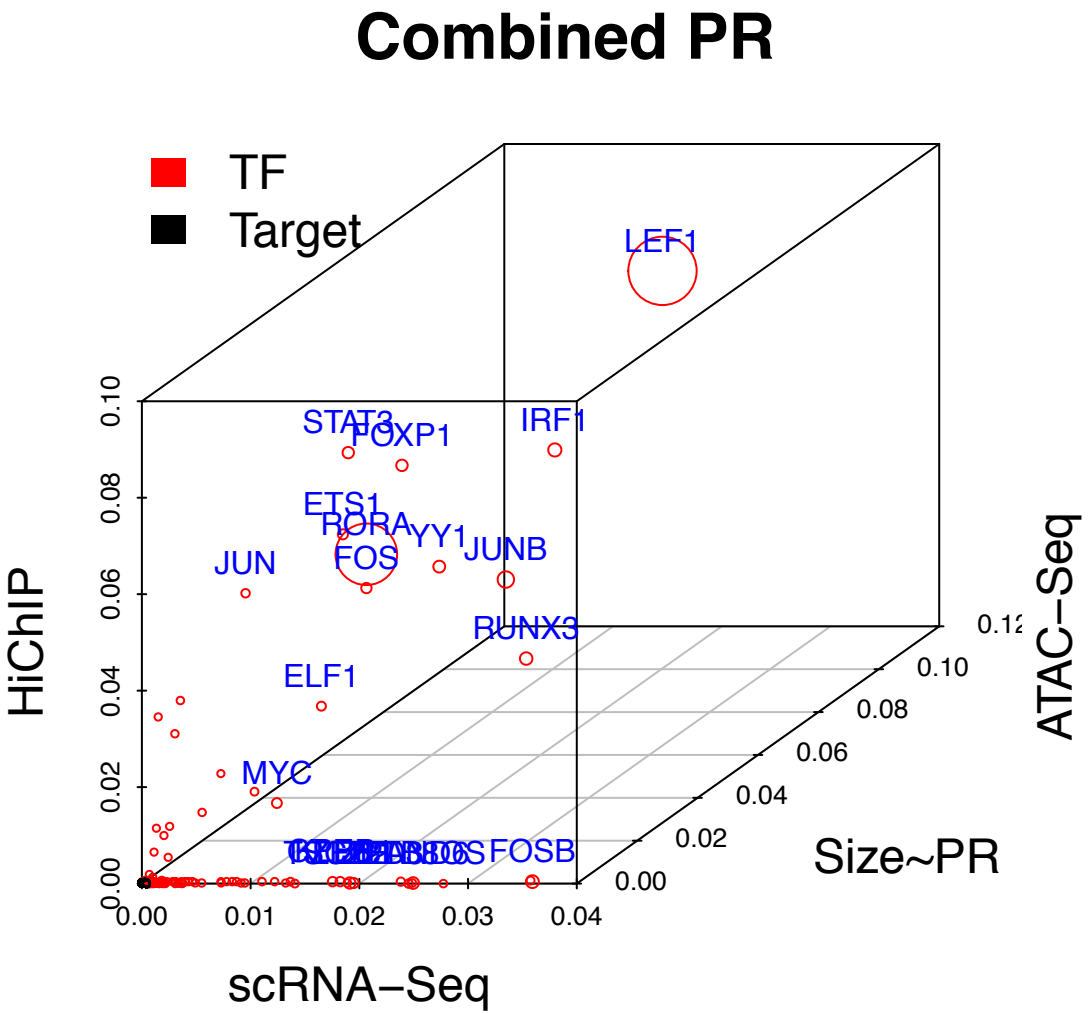
Combined PR
TF
Target
LEF1
STAT3
FOXP1
IRF1
ETS1
RORA
YY1
JUN
FOS
JUNB
RUNX3
ELF1
MYC
FOSB
HiChIP
scRNA−Seq
ATAC−Seq
Size~PR
0.00
0.01
0.02
0.03
0.04
0.10
0.08
0.06
0.04
0.02
0.00
0.12

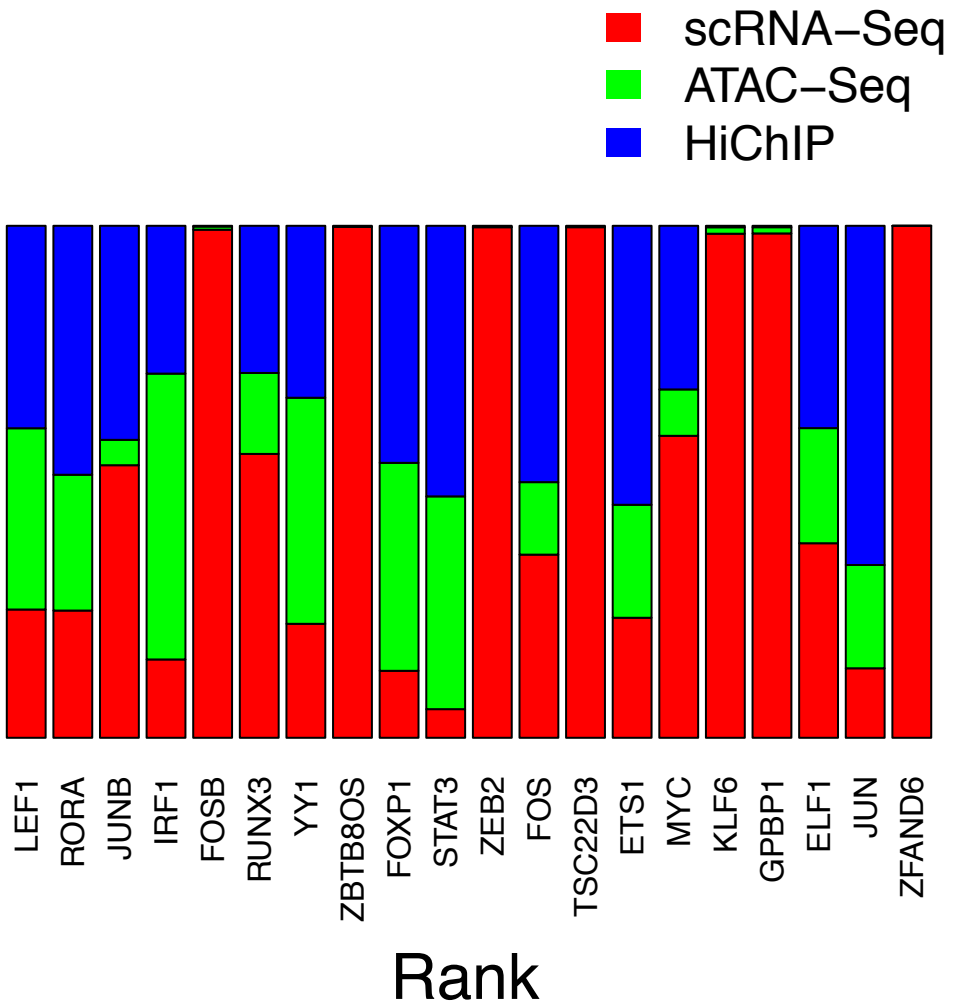
scRNA−Seq
ATAC−Seq
HiChIP
LEF1
RORA
JUNB
IRF1
FOSB
RUNX3
YY1
ZBTB8OS
FOXP1
STAT3
ZEB2
FOS
TSC22D3
ETS1
MYC
KLF6
GPBP1
ELF1
JUN
ZFAND6
Rank

Figure S6

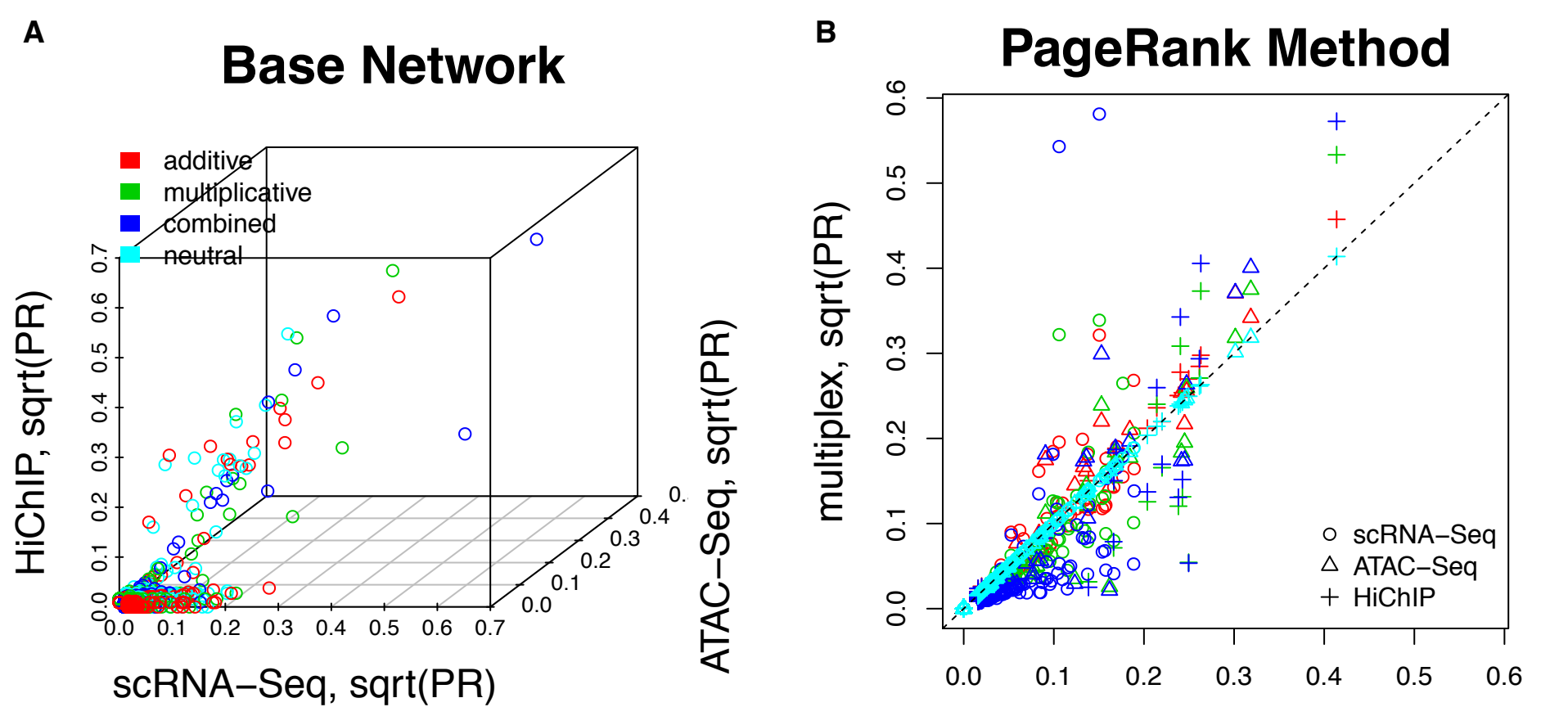
A
Base Network
additive
multiplicative
combined
neutral
HiChIP, sqrt(PR)
scRNA−Seq, sqrt(PR)
ATAC−Seq, sqrt(PR)
B
PageRank Method
multiplex, sqrt(PR)
regular, sqrt(PR)
scRNA−Seq
ATAC−Seq
HiChIP

Figure S7

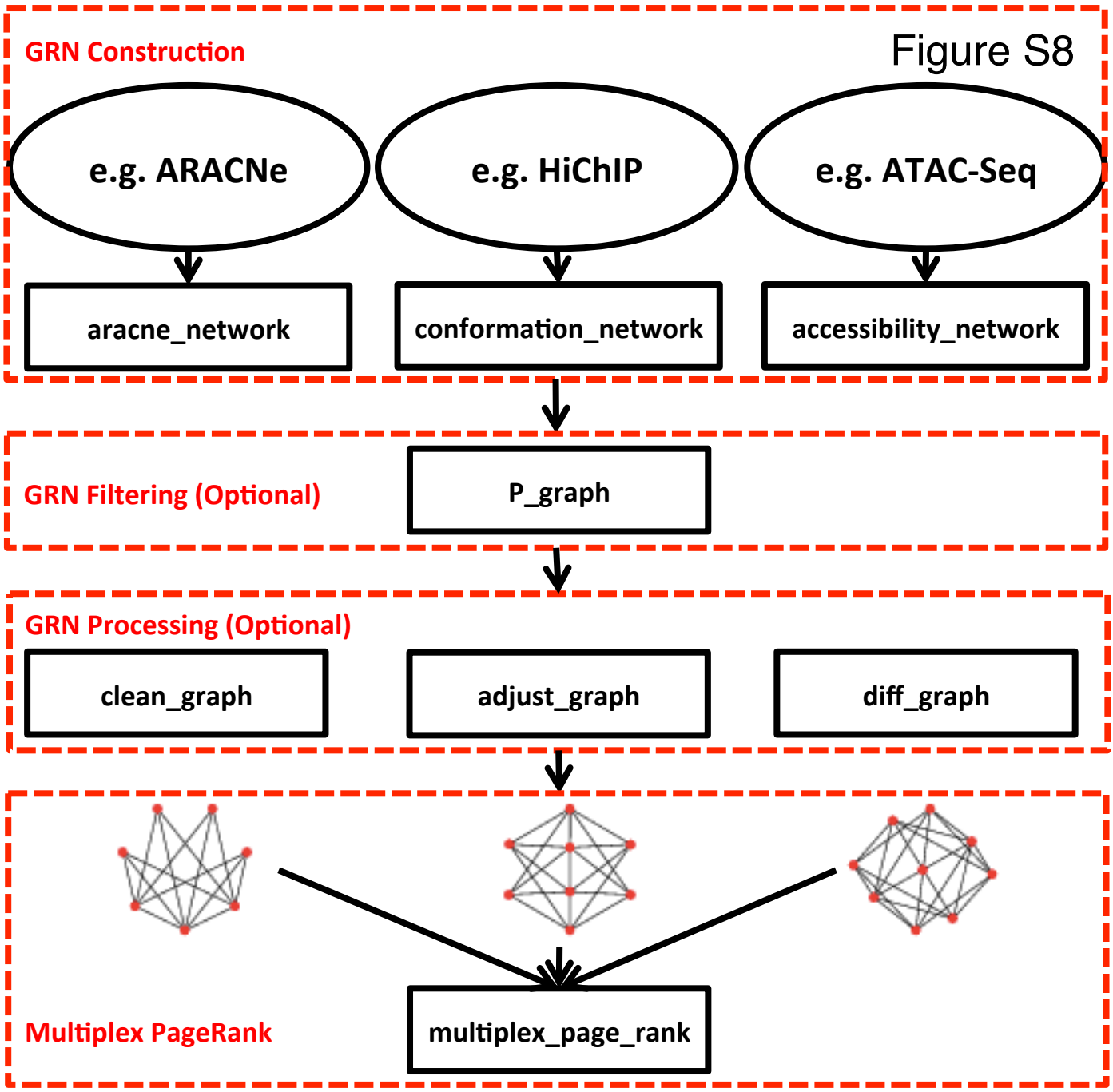

- aracne_network: re-format ARACNe regulon R object.
- accessibility_network: generate genome accessibility-based GRNs from called peaks.
- conformation_network: generate chromosome conformation-based GRNs from records.
- P_graph: filter GRNs by probability-based approaches, with interaction confidence and mode as edge attributes, and regular PageRank as vertex attribute.
- clean_graph: remove vertex by corresponding sub-graph size, name and PageRank, with updated regular PageRank as vertex attribute.
- adjust_graph: re-calculate PageRank with weight, personalization and damping.
- diff_graph: calculate differential graph, with mode of changing as edge attribute, and regular PageRank as vertex attribute.
- multiplex_page_rank: calculate multiplex PageRank from different networks.

accessibility_network

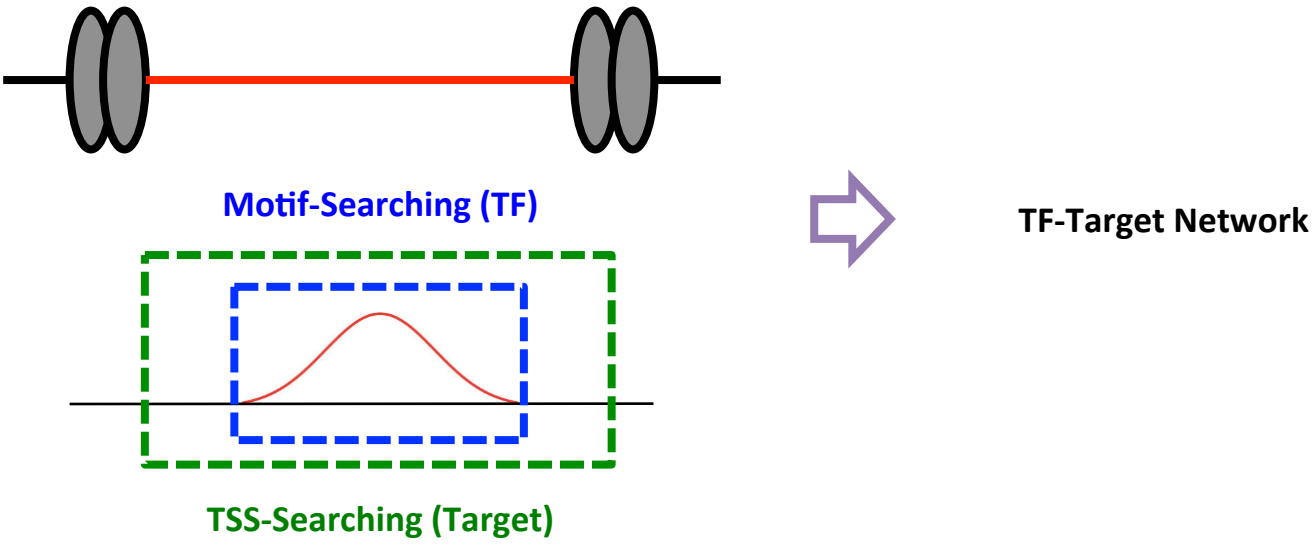

conformation_network

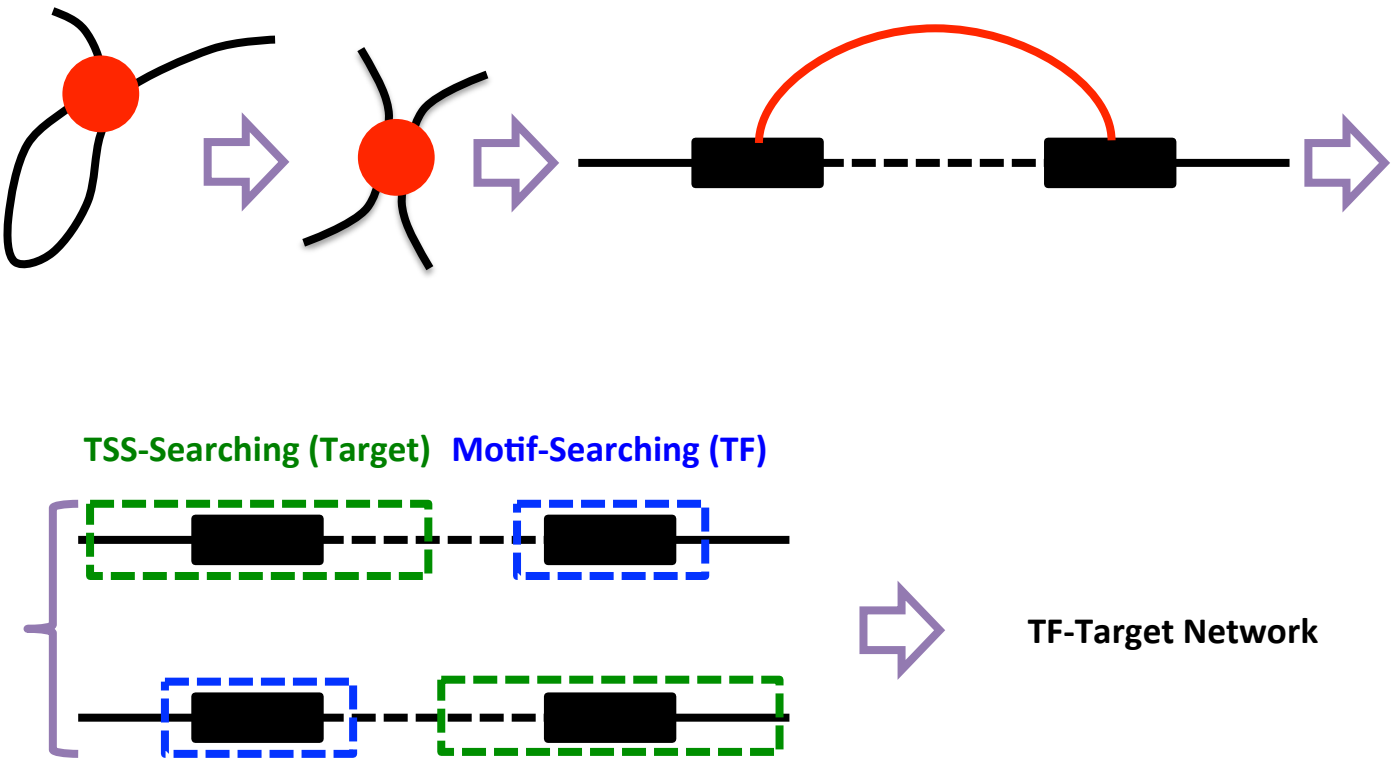

Figure S9

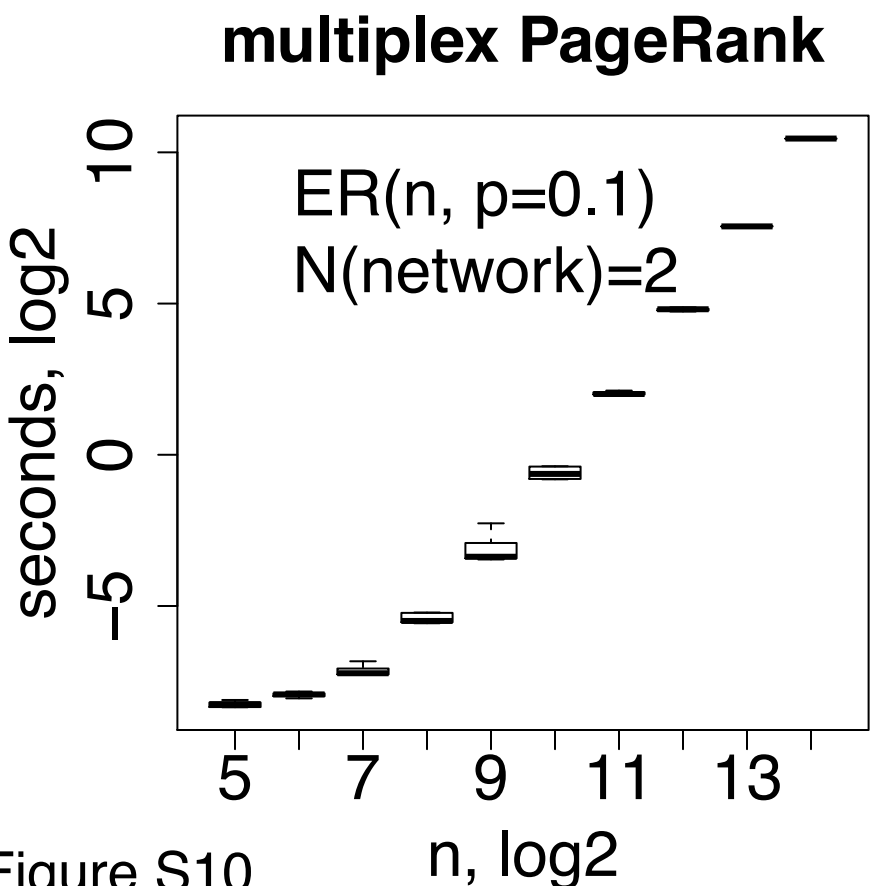
multiplex PageRank
ER(n, p=0.1)
N(network)=2
seconds, log2
−5
0
5
10
5
7
9
11
13
n, log2

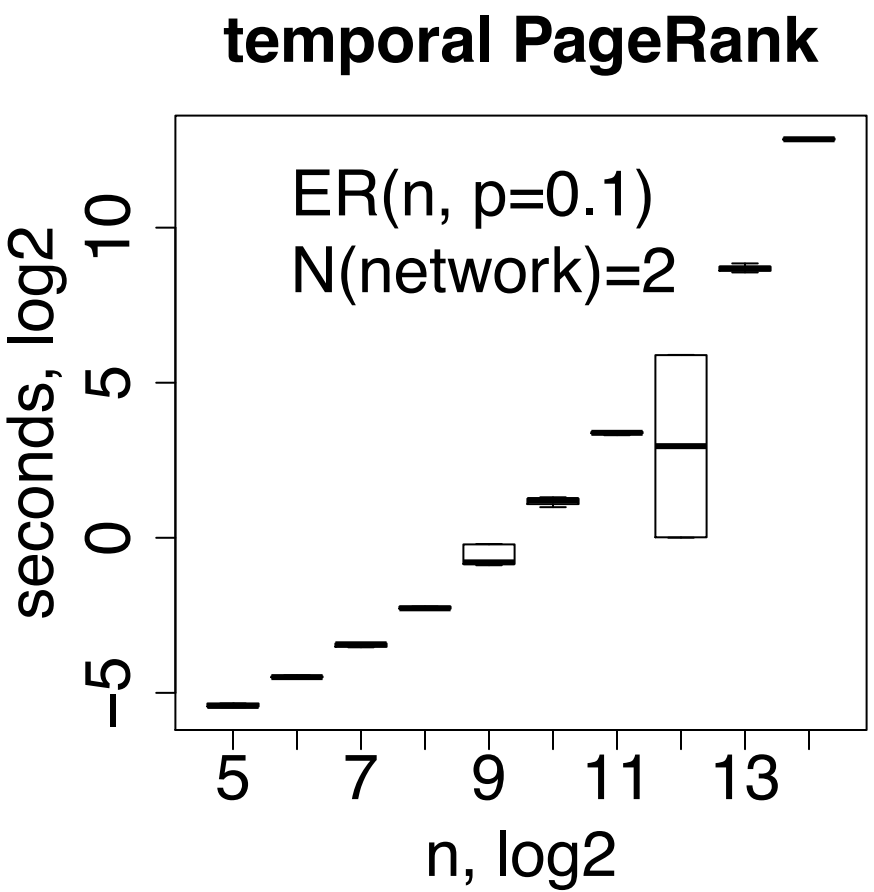
temporal PageRank
ER(n, p=0.1)
N(network)=2
seconds, log2
−5
0
5
10
5
7
9
11
13
n, log2

Figure S10

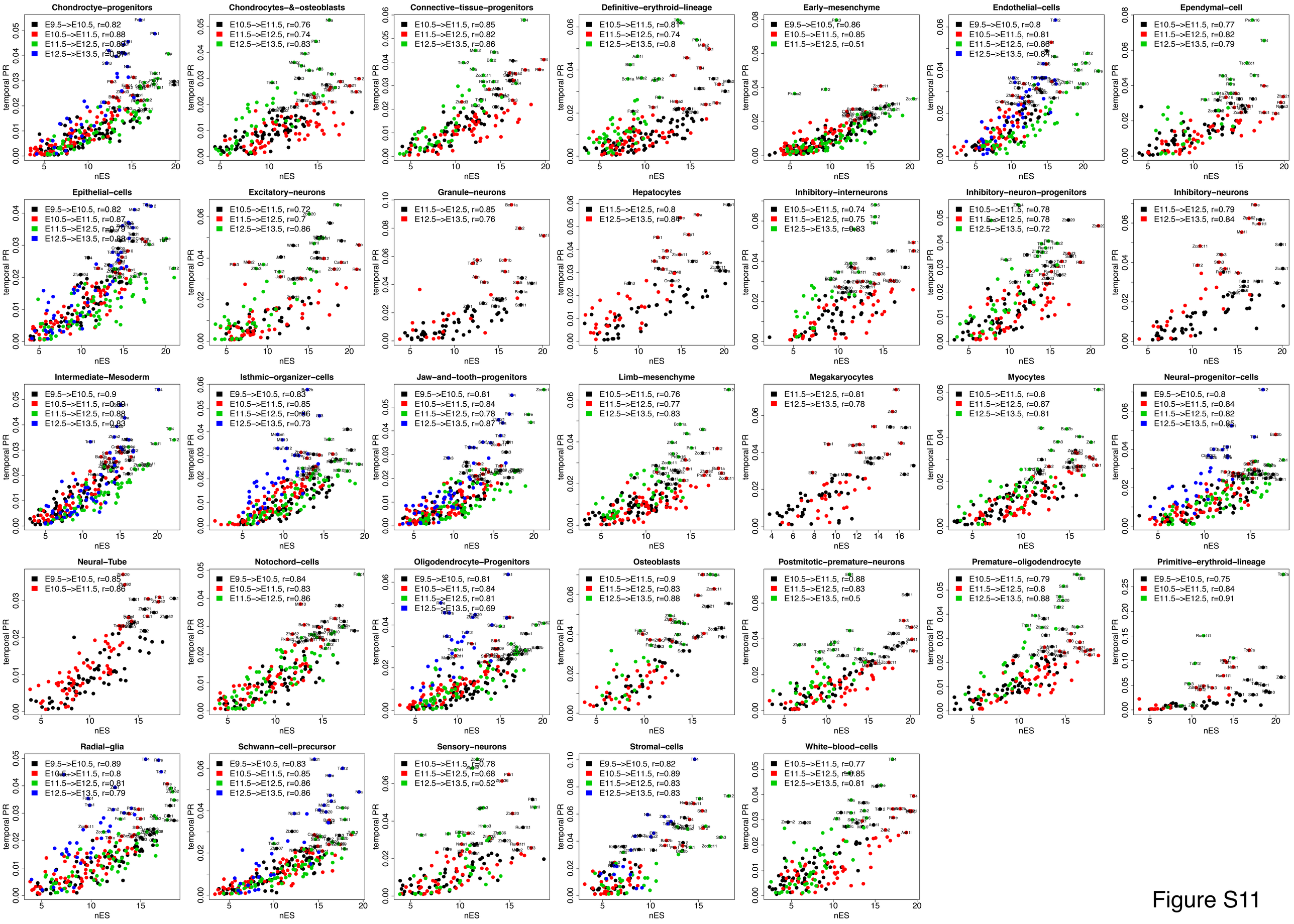
Chondroctye−progenitors
E9.5−>E10.5, r=0.82
E10.5−>E11.5, r=0.88
E11.5−>E12.5, r=0.86
E12.5−>E13.5, r=0.87
Chondrocytes−&−osteoblasts
E10.5−>E11.5, r=0.76
E11.5−>E12.5, r=0.74
E12.5−>E13.5, r=0.83
Connective−tissue−progenitors
E10.5−>E11.5, r=0.85
E11.5−>E12.5, r=0.82
E12.5−>E13.5, r=0.86
Definitive−erythroid−lineage
E10.5−>E11.5, r=0.81
E11.5−>E12.5, r=0.74
E12.5−>E13.5, r=0.8
Early−mesenchyme
E9.5−>E10.5, r=0.86
E10.5−>E11.5, r=0.85
E11.5−>E12.5, r=0.51
Endothelial−cells
E9.5−>E10.5, r=0.8
E10.5−>E11.5, r=0.81
E11.5−>E12.5, r=0.86
E12.5−>E13.5, r=0.87
Ependymal−cell
E10.5−>E11.5, r=0.77
E11.5−>E12.5, r=0.82
E12.5−>E13.5, r=0.79
Epithelial−cells
E9.5−>E10.5, r=0.82
E10.5−>E11.5, r=0.87
E11.5−>E12.5, r=0.79
E12.5−>E13.5, r=0.83
Excitatory−neurons
E10.5−>E11.5, r=0.72
E11.5−>E12.5, r=0.7
E12.5−>E13.5, r=0.86
Granule−neurons
E11.5−>E12.5, r=0.85
E12.5−>E13.5, r=0.76
Hepatocytes
E11.5−>E12.5, r=0.8
E12.5−>E13.5, r=0.84
Inhibitory−interneurons
E10.5−>E11.5, r=0.74
E11.5−>E12.5, r=0.75
E12.5−>E13.5, r=0.83
Inhibitory−neuron−progenitors
E10.5−>E11.5, r=0.78
E11.5−>E12.5, r=0.78
E12.5−>E13.5, r=0.72
Inhibitory−neurons
E11.5−>E12.5, r=0.79
E12.5−>E13.5, r=0.84
Intermediate−Mesoderm
E9.5−>E10.5, r=0.9
E10.5−>E11.5, r=0.89
E11.5−>E12.5, r=0.88
E12.5−>E13.5, r=0.83
Isthmic−organizer−cells
E9.5−>E10.5, r=0.83
E10.5−>E11.5, r=0.85
E11.5−>E12.5, r=0.86
E12.5−>E13.5, r=0.73
Jaw−and−tooth−progenitors
E9.5−>E10.5, r=0.81
E10.5−>E11.5, r=0.84
E11.5−>E12.5, r=0.78
E12.5−>E13.5, r=0.87
Limb−mesenchyme
E10.5−>E11.5, r=0.76
E11.5−>E12.5, r=0.77
E12.5−>E13.5, r=0.83
Megakaryocytes
E11.5−>E12.5, r=0.81
E12.5−>E13.5, r=0.78
Myocytes
E10.5−>E11.5, r=0.8
E11.5−>E12.5, r=0.87
E12.5−>E13.5, r=0.81
Neural−progenitor−cells
E9.5−>E10.5, r=0.8
E10.5−>E11.5, r=0.84
E11.5−>E12.5, r=0.82
E12.5−>E13.5, r=0.85
Neural−Tube
E9.5−>E10.5, r=0.85
E10.5−>E11.5, r=0.86
Notochord−cells
E9.5−>E10.5, r=0.84
E10.5−>E11.5, r=0.83
E11.5−>E12.5, r=0.86
Oligodendrocyte−Progenitors
E9.5−>E10.5, r=0.81
E10.5−>E11.5, r=0.84
E11.5−>E12.5, r=0.81
E12.5−>E13.5, r=0.69
Osteoblasts
E10.5−>E11.5, r=0.9
E11.5−>E12.5, r=0.83
E12.5−>E13.5, r=0.88
Postmitotic−premature−neurons
E10.5−>E11.5, r=0.88
E11.5−>E12.5, r=0.83
E12.5−>E13.5, r=0.5
Premature−oligodendrocyte
E10.5−>E11.5, r=0.79
E11.5−>E12.5, r=0.8
E12.5−>E13.5, r=0.88
Primitive−erythroid−lineage
E9.5−>E10.5, r=0.75
E10.5−>E11.5, r=0.84
E11.5−>E12.5, r=0.91
Radial−glia
E9.5−>E10.5, r=0.89
E10.5−>E11.5, r=0.8
E11.5−>E12.5, r=0.81
E12.5−>E13.5, r=0.79
Schwann−cell−precursor
E9.5−>E10.5, r=0.83
E10.5−>E11.5, r=0.85
E11.5−>E12.5, r=0.86
E12.5−>E13.5, r=0.86
Sensory−neurons
E10.5−>E11.5, r=0.78
E11.5−>E12.5, r=0.68
E12.5−>E13.5, r=0.52
Stromal−cells
E9.5−>E10.5, r=0.82
E10.5−>E11.5, r=0.89
E11.5−>E12.5, r=0.83
E12.5−>E13.5, r=0.83
White−blood−cells
E10.5−>E11.5, r=0.77
E11.5−>E12.5, r=0.85
E12.5−>E13.5, r=0.81
temporal PR
nES

Figure S11

Table S1

Analysis Type: PANTHER Overrepresentation Test (Released 20200728)
Annotation Version and Release Date: GO Ontology database DOI: 10.5281/zenodo.4033054 Released 2020-09-10
Analyzed List: upload_1 (Homo sapiens)
Reference List: Homo sapiens (all genes in database)
Test Type: FISHER
Correction: FDR

GO biological process complete	Homo sapiens - REFLIST (20851)	upload_1 (20)	upload_1 (expected)	upload_1 (over/under)	upload_1 (fold Enrichment)	upload_1 (raw P-value)	upload_1 (FDR)
T-helper 17 cell differentiation (GO:0072539)	9	2	.01	+	> 100	4.77E-05	5.06E-03
T-helper 17 type immune response (GO:0072538)	10	2	.01	+	> 100	5.72E-05	5.80E-03
radial glial cell differentiation (GO:0060019)	13	2	.01	+	> 100	9.09E-05	8.76E-03
regulation of monocyte differentiation (GO:0045655)	20	3	.02	+	> 100	1.32E-06	2.41E-04
CD4-positive, alpha-beta T cell differentiation involved in immune response (GO:0002294)	29	4	.03	+	> 100	2.46E-08	9.56E-06
T-helper cell differentiation (GO:0042093)	29	4	.03	+	> 100	2.46E-08	9.33E-06
positive regulation of ATP biosynthetic process (GO:2001171)	15	2	.01	+	> 100	1.18E-04	1.09E-02
alpha-beta T cell differentiation involved in immune response (GO:0002293)	30	4	.03	+	> 100	2.79E-08	9.65E-06
alpha-beta T cell activation involved in immune response (GO:0002287)	30	4	.03	+	> 100	2.79E-08	9.45E-06
T cell differentiation involved in immune response (GO:0002292)	34	4	.03	+	> 100	4.43E-08	1.36E-05
positive regulation by host of viral transcription (GO:0043923)	17	2	.02	+	> 100	1.48E-04	1.31E-02
regulation of CD8-positive, alpha-beta T cell activation (GO:2001185)	18	2	.02	+	> 100	1.64E-04	1.42E-02
CD4-positive, alpha-beta T cell differentiation (GO:0043367)	39	4	.04	+	> 100	7.39E-08	2.06E-05
regulation of ATP biosynthetic process (GO:2001169)	20	2	.02	+	> 100	1.99E-04	1.68E-02
positive regulation of pri-miRNA transcription by RNA polymerase II (GO:1902895)	41	4	.04	+	> 100	8.91E-08	2.32E-05
response to corticosterone (GO:0051412)	211	2	.02	+	99.29	2.18E-04	1.81E-02
regulation of pri-miRNA transcription by RNA polymerase II (GO:1902893)	53	5	.05	+	98.35	2.09E-09	1.01E-06
hypothalamus development (GO:0021854)	22	2	.02	+	94.78	2.38E-04	1.94E-02
alpha-beta T cell differentiation (GO:0046632)	56	5	.05	+	93.08	2.70E-09	1.26E-06
CD4-positive, alpha-beta T cell activation (GO:0035710)	45	4	.04	+	92.67	1.26E-07	3.04E-05
cellular response to growth hormone stimulus (GO:0071378)	23	2	.02	+	90.66	2.58E-04	2.09E-02
response to muscle stretch (GO:0035994)	24	2	.02	+	86.88	2.80E-04	2.28E-02
positive regulation of purine nucleotide biosynthetic process (GO:1900373)	25	2	.02	+	83.40	3.02E-04	2.34E-02
positive regulation of nucleotide biosynthetic process (GO:0030810)	25	2	.02	+	83.40	3.02E-04	2.33E-02
regulation of B cell receptor signaling pathway (GO:0050855)	26	2	.02	+	80.20	3.25E-04	2.44E-02
alpha-beta T cell activation (GO:0046631)	69	5	.07	+	75.55	7.26E-09	3.04E-06
beta-catenin-TCF complex assembly (GO:1904837)	29	2	.03	+	71.90	3.99E-04	2.91E-02
negative regulation of lymphocyte apoptotic process (GO:0070229)	31	2	.03	+	67.26	4.52E-04	3.21E-02
positive regulation of erythrocyte differentiation (GO:0045648)	32	2	.03	+	65.16	4.80E-04	3.37E-02
response to mineralocorticoid (GO:0051385)	33	2	.03	+	63.18	5.09E-04	3.54E-02
T cell activation involved in immune response (GO:0002286)	67	4	.06	+	62.24	5.72E-07	1.15E-04
response to growth hormone (GO:0060416)	36	2	.03	+	57.92	6.01E-04	4.10E-02
positive regulation of myeloid leukocyte differentiation (GO:0002763)	58	3	.06	+	53.93	2.61E-05	3.13E-03
cellular response to cadmium ion (GO:0071276)	39	2	.04	+	53.46	7.00E-04	4.66E-02
positive regulation of myeloid cell differentiation (GO:0045639)	100	5	.10	+	52.13	4.27E-08	1.33E-05
cellular response to calcium ion (GO:0071277)	85	4	.08	+	49.06	1.42E-06	2.57E-04
regulation of myeloid leukocyte differentiation (GO:0002761)	123	5	.12	+	42.38	1.16E-07	2.83E-05
neural precursor cell proliferation (GO:0061351)	75	3	.07	+	41.70	5.47E-05	5.65E-03
diencephalon development (GO:0021536)	77	3	.07	+	40.62	5.90E-05	5.86E-03
lymphocyte activation involved in immune response (GO:0002285)	112	4	.11	+	37.23	4.10E-06	6.39E-04
limbic system development (GO:0021761)	113	4	.11	+	36.90	4.24E-06	6.48E-04
T cell differentiation (GO:0030217)	147	5	.14	+	35.46	2.72E-07	5.85E-05
positive regulation of smooth muscle cell proliferation (GO:0048661)	90	3	.09	+	34.75	9.24E-05	8.86E-03
myeloid leukocyte differentiation (GO:0002573)	123	4	.12	+	33.90	5.87E-06	8.73E-04
response to cAMP (GO:0051591)	98	3	.09	+	31.91	1.18E-04	1.09E-02
positive regulation of hemopoiesis (GO:1903708)	201	6	.19	+	31.12	3.06E-08	1.01E-05
regulation of myeloid cell differentiation (GO:0045637)	238	7	.23	+	30.66	1.92E-09	9.54E-07
negative regulation of leukocyte differentiation (GO:1902106)	104	3	.10	+	30.07	1.40E-04	1.25E-02
response to calcium ion (GO:0051592)	152	4	.15	+	27.44	1.33E-05	1.70E-03
modulation of process of other organism involved in symbiotic interaction (GO:0051817)	116	3	.11	+	26.96	1.92E-04	1.63E-02
positive regulation of leukocyte differentiation (GO:1902107)	158	4	.15	+	26.39	1.54E-05	1.96E-03
regulation of leukocyte differentiation (GO:1902105)	289	7	.28	+	25.25	7.12E-09	3.06E-06
lymphocyte differentiation (GO:0030098)	248	6	.24	+	25.22	1.03E-07	2.60E-05
regulation of DNA binding (GO:0051101)	130	3	.12	+	24.06	2.66E-04	2.12E-02
cellular response to reactive oxygen species (GO:0034614)	132	3	.13	+	23.69	2.78E-04	2.20E-02
leukocyte differentiation (GO:0002521)	354	8	.34	+	23.56	7.97E-10	4.69E-07
modulation of process of other organism (GO:0035821)	133	3	.13	+	23.52	2.84E-04	2.22E-02
response to mechanical stimulus (GO:0009612)	223	5	.21	+	23.38	2.02E-06	3.49E-04
regulation of smooth muscle cell proliferation (GO:0048660)	139	3	.13	+	22.50	+	3.23E-04 2.45E-02
response to organophosphorus (GO:0046683)	139	3	.13	+	22.50	3.23E-04	2.43E-02
female pregnancy (GO:0007565)	188	4	.18	+	22.18	3.00E-05	3.53E-03
negative regulation of hemopoiesis (GO:1903707)	142	3	.14	+	21.43	3.43E-04	2.55E-02
response to estradiol (GO:0032355)	146	3	.14	+	21.42	3.72E-04	2.74E-02
cellular response to metal ion (GO:0071248)	195	4	.19	+	21.39	3.45E-05	3.92E-03
T cell activation (GO:0042110)	246	5	.24	+	21.19	3.23E-06	5.25E-04
positive regulation of epithelial cell migration (GO:0010634)	148	3	.14	+	21.13	3.87E-04	2.83E-02
response to interleukin-1 (GO:0070555)	201	4	.19	+	20.75	3.87E-05	4.22E-03
regulation of T cell differentiation (GO:0045580)	151	3	.14	+	20.71	4.10E-04	2.96E-02
response to purine-containing compound (GO:0014074)	155	3	.15	+	20.18	4.41E-04	3.15E-02
regulation of hemopoiesis (GO:1903706)	472	9	.45	+	19.88	2.28E-10	1.51E-07
response to transforming growth factor beta (GO:0071559)	158	3	.15	+	19.80	+	4.66E-04 3.30E-02
multi-multicellular organism process (GO:0044706)	221	4	.21	+	18.87	5.56E-05	5.71E-03
cellular response to inorganic substance (GO:0071241)	223	4	.21	+	18.70	5.76E-05	5.80E-03
transcription by RNA polymerase II (GO:0006366)	409	7	.39	+	17.84	7.36E-08	2.09E-05
cellular response to interleukin-1 (GO:0071347)	176	3	.17	+	17.77	6.35E-04	4.32E-02
myeloid cell differentiation (GO:0030099)	235	4	.23	+	17.75	7.03E-05	6.95E-03
regulation of lymphocyte differentiation (GO:0045619)	181	3	.17	+	17.28	6.88E-04	4.64E-02
negative regulation of cell-cell adhesion (GO:0022408)	185	3	.18	+	16.91	7.32E-04	4.83E-02
response to alcohol (GO:0097305)	254	4	.24	+	16.42	9.46E-05	9.01E-03
lymphocyte activation (GO:0046649)	394	6	.38	+	15.88	1.47E-06	2.68E-04
hemopoiesis (GO:0030097)	592	9	.57	+	15.85	1.62E-09	8.61E-07
transcription, DNA-templated (GO:0006351)	558	8	.54	+	14.95	2.63E-08	9.51E-06
nucleic acid-templated transcription (GO:0097659)	559	8	.54	+	14.92	2.67E-08	9.43E-06
hematopoietic or lymphoid organ development (GO:0048534)	640	9	.61	+	14.66	3.18E-09	1.45E-06
RNA biosynthetic process (GO:0032774)	572	8	.55	+	14.58	3.18E-08	1.01E-05
cellular response to chemical stress (GO:0062197)	292	4	.28	+	14.28	1.61E-04	1.40E-02
immune system development (GO:0002520)	675	9	.65	+	13.90	5.03E-09	2.22E-06
response to drug (GO:0042493)	402	5	.39	+	12.97	3.35E-05	3.83E-03
regulation of leukocyte cell-cell adhesion (GO:1903037)	322	4	.31	+	12.95	2.32E-04	1.91E-02
angiogenesis (GO:0001525)	322	4	.31	+	12.95	2.32E-04	1.90E-02
cell population proliferation (GO:0008283)	496	6	.48	+	12.61	5.47E-06	8.20E-04
blood vessel morphogenesis (GO:0048514)	415	5	.40	+	12.56	3.89E-05	4.21E-03
positive regulation of transcription by RNA polymerase II (GO:0045944)	1278	15	1.23	+	12.24	8.12E-15	1.44E-11
response to lipid (GO:0033993)	857	10	.82	+	12.17	1.84E-09	9.44E-07
regulation of epithelial cell proliferation (GO:0050678)	346	4	.33	+	12.05	3.05E-04	2.34E-02
positive regulation of cell migration (GO:0030335)	528	6	.51	+	11.85	7.79E-06	1.13E-03
response to inorganic substance (GO:0010035)	548	6	.53	+	11.41	9.61E-06	1.36E-03
positive regulation of cell motility (GO:2000147)	551	6	.53	+	11.35	9.91E-06	1.37E-03
response to metal ion (GO:0010038)	375	4	.36	+	11.12	4.12E-04	2.96E-02
positive regulation of transcription, DNA-templated (GO:0045893)	1601	17	1.54	+	11.07	1.11E-16	1.77E-12
positive regulation of locomotion (GO:0040017)	567	6	.54	+	11.03	1.16E-05	1.53E-03
positive regulation of cellular component movement (GO:0051272)	569	6	.55	+	10.99	1.19E-05	1.55E-03
tube morphogenesis (GO:0035239)	668	7	.64	+	10.92	1.93E-06	3.37E-04
positive regulation of nucleic acid-templated transcription (GO:1903508)	1686	17	1.62	+	10.51	2.63E-16	2.09E-12
positive regulation of RNA biosynthetic process (GO:1902680)	1687	17	1.62	+	10.51	2.66E-16	1.41E-12
forebrain development (GO:0030900)	404	4	.39	+	10.32	5.44E-04	3.76E-02
blood vessel development (GO:0001568)	505	5	.48	+	10.32	9.77E-05	9.09E-03
response to cytokine (GO:0034097)	1131	11	1.08	+	10.14	1.34E-09	7.33E-07
positive regulation of RNA metabolic process (GO:0051254)	1780	17	1.71	+	9.96	6.49E-16	2.58E-12
gland development (GO:0048732)	422	4	.40	+	9.88	6.40E-04	4.33E-02
vasculature development (GO:0001944)	528	5	.51	+	9.87	1.20E-04	1.10E-02
regulation of cytokine production (GO:0001817)	741	7	.71	+	9.85	3.81E-06	6.11E-04
response to growth factor (GO:0070848)	533	5	.51	+	9.78	1.26E-04	1.14E-02
cellular response to hormone stimulus (GO:0032870)	537	5	.52	+	9.71	1.30E-04	1.18E-02
negative regulation of transcription by RNA polymerase II (GO:0000122)	970	9	.93	+	9.67	1.12E-07	2.77E-05
regulation of cell-cell adhesion (GO:0022407)	432	4	.41	+	9.65	6.98E-04	4.68E-02
positive regulation of cell differentiation (GO:0045597)	1012	9	.97	+	9.27	1.60E-07	3.63E-05
response to organic cyclic compound (GO:0014070)	905	8	.87	+	9.22	1.02E-06	1.89E-04
positive regulation of macromolecule biosynthetic process (GO:0010557)	1930	17	1.85	+	9.18	2.50E-15	7.94E-12
positive regulation of nucleobase-containing compound metabolic process (GO:0045935)	1953	17	1.87	+	9.07	3.04E-15	8.06E-12
cellular response to cytokine stimulus (GO:0071345)	1041	9	1.00	+	9.01	2.03E-07	4.48E-05
cytokine-mediated signaling pathway (GO:0019221)	701	6	.67	+	8.92	3.82E-05	4.22E-03
negative regulation of cell population proliferation (GO:0008285)	702	6	.67	+	8.91	3.85E-05	4.22E-03
positive regulation of cellular biosynthetic process (GO:0031328)	2031	17	1.95	+	8.73	5.83E-15	1.32E-11
negative regulation of cell differentiation (GO:0045596)	724	6	.69	+	8.64	4.57E-05	4.87E-03
positive regulation of biosynthetic process (GO:0009891)	2066	17	1.98	+	8.58	7.74E-15	1.54E-11
tube development (GO:0035295)	870	7	.83	+	8.39	1.88E-05	1.46E-03
negative regulation of immune system process (GO:0002683)	624	5	.60	+	8.35	2.60E-04	2.08E-02
nucleobase-containing compound biosynthetic process (GO:0034654)	1010	8	.97	+	8.26	2.32E-06	3.93E-04
negative regulation of transcription, DNA-templated (GO:0045892)	1310	10	1.26	+	7.96	1.02E-07	2.61E-05
response to abiotic stimulus (GO:0009628)	1186	9	1.14	+	7.91	6.07E-07	1.21E-04
leukocyte activation (GO:0045321)	935	7	.90	+	7.81	1.72E-05	2.16E-03
negative regulation of nucleic acid-templated transcription (GO:1903507)	1351	10	1.30	+	7.72	1.36E-07	3.23E-05
negative regulation of RNA biosynthetic process (GO:1902679)	1353	10	1.30	+	7.71	1.38E-07	3.22E-05
heterocycle biosynthetic process (GO:0018130)	1083	8	1.04	+	7.70	3.90E-06	6.13E-04
aromatic compound biosynthetic process (GO:0019438)	1094	8	1.05	+	7.62	4.20E-06	6.48E-04
response to hormone (GO:0009725)	828	6	.79	+	7.55	9.58E-05	9.01E-03
positive regulation of gene expression (GO:0010628)	2372	17	2.28	+	7.47	7.66E-14	1.22E-10
negative regulation of developmental process (GO:0051093)	984	7	.94	+	7.42	2.40E-05	2.91E-03
regulation of cell differentiation (GO:0045595)	1884	13	1.81	+	7.19	1.17E-09	6.64E-07
regulation of immune system process (GO:0002682)	1741	12	1.67	+	7.19	7.91E-09	3.22E-06
negative regulation of RNA metabolic process (GO:0051253)	1455	10	1.40	+	7.17	2.71E-07	5.91E-05
negative regulation of cell death (GO:0060548)	1027	7	.99	+	7.11	3.15E-05	3.66E-03
multi-organism reproductive process (GO:0044703)	1029	7	.99	+	7.09	3.19E-05	3.68E-03
regulation of cell migration (GO:0030334)	891	6	.85	+	7.02	1.43E-04	1.27E-02
anatomical structure formation involved in morphogenesis (GO:0048646)	897	6	.86	+	6.97	1.48E-04	1.30E-02
negative regulation of cellular macromolecule biosynthetic process (GO:2000113)	1512	10	1.45	+	6.90	3.87E-07	8.11E-05
regulation of cell cycle (GO:0051726)	1210	8	1.16	+	6.89	8.81E-06	1.24E-03
negative regulation of apoptotic process (GO:0043066)	915	6	.88	+	6.84	1.65E-04	1.42E-02
organic cyclic compound biosynthetic process (GO:1901362)	1231	8	1.18	+	6.78	9.99E-06	1.37E-03
cell activation (GO:0001775)	1082	7	1.04	+	6.74	4.39E-05	4.72E-03
brain development (GO:0007420)	775	5	.74	+	6.73	6.99E-04	4.67E-02
negative regulation of programmed cell death (GO:0043069)	933	6	.89	+	6.70	1.84E-04	1.57E-02
negative regulation of macromolecule biosynthetic process (GO:0010558)	1566	10	1.50	+	6.66	5.36E-07	1.11E-04
multi-organism process (GO:0051704)	1097	7	1.05	+	6.65	4.80E-05	5.05E-03
negative regulation of nucleobase-containing compound metabolic process (GO:0045934)	1572	10	1.51	+	6.63	5.55E-07	1.13E-04
positive regulation of developmental process (GO:0051094)	1415	9	1.36	+	6.63	2.63E-06	4.32E-04
positive regulation of cell population proliferation (GO:0008284)	946	6	.91	+	6.61	1.98E-04	1.68E-02
positive regulation of immune system process (GO:0002684)	1106	7	1.06	+	6.60	5.05E-05	5.29E-03
regulation of cell motility (GO:2000145)	952	6	.91	+	6.57	2.05E-04	1.72E-02
negative regulation of cellular biosynthetic process (GO:0031327)	1626	10	1.56	+	6.41	7.58E-07	1.47E-04
positive regulation of multicellular organismal process (GO:0051240)	1797	11	1.72	+	6.38	1.61E-07	3.60E-05
regulation of transcription by RNA polymerase II (GO:0006357)	2628	16	2.52	+	6.35	1.24E-11	1.23E-08
regulation of locomotion (GO:0040012)	994	6	.95	+	6.29	2.59E-04	2.08E-02
negative regulation of biosynthetic process (GO:0009890)	1657	10	1.59	+	6.29	9.02E-07	1.69E-04
central nervous system development (GO:0007417)	1025	6	.98	+	6.10	3.05E-04	2.33E-02
regulation of cellular component movement (GO:0051270)	1042	6	1.00	+	6.00	3.33E-04	2.49E-02
response to oxygen-containing compound (GO:1901700)	1610	9	1.54	+	5.83	7.60E-06	1.11E-03
response to endogenous stimulus (GO:0009719)	1436	8	1.38	+	5.81	3.06E-05	3.57E-03
RNA metabolic process (GO:0016070)	1621	9	1.55	+	5.79	8.84E-06	1.15E-03
cellular response to oxygen-containing compound (GO:1901701)	1081	6	1.04	+	5.79	4.06E-04	2.95E-02
reproductive process (GO:0022414)	1471	8	1.41	+	5.67	3.63E-05	4.07E-03
reproduction (GO:0000003)	1474	8	1.41	+	5.66	3.69E-05	4.10E-03
regulation of cell population proliferation (GO:0042127)	1677	9	1.61	+	5.60	1.06E-05	1.44E-03
regulation of cell death (GO:0010941)	1722	9	1.65	+	5.45	1.31E-05	1.70E-03
regulation of multicellular organismal development (GO:2000026)	2107	11	2.02	+	5.44	8.06E-07	1.55E-04
positive regulation of nitrogen compound metabolic process (GO:0051173)	3267	17	3.13	+	5.42	1.51E-11	1.42E-08
regulation of transcription, DNA-templated (GO:0006355)	3462	18	3.32	+	5.42	1.29E-12	1.87E-09
cellular response to endogenous stimulus (GO:0071495)	1160	6	1.11	+	5.39	5.91E-04	4.05E-02
regulation of nucleic acid-templated transcription (GO:1903506)	3531	18	3.39	+	5.31	1.83E-12	2.42E-09
cellular nitrogen compound biosynthetic process (GO:0044271)	1571	8	1.51	+	5.31	5.82E-05	5.82E-03
regulation of RNA biosynthetic process (GO:2001141)	3536	18	3.39	+	5.31	1.87E-12	2.29E-09
positive regulation of cellular metabolic process (GO:0031325)	3454	17	3.31	+	5.13	3.77E-11	2.86E-08
nucleic acid metabolic process (GO:0090304)	2237	11	2.15	+	5.13	1.47E-06	2.63E-04
cellular macromolecule biosynthetic process (GO:0034645)	1639	8	1.57	+	5.09	7.86E-05	7.67E-03
regulation of developmental process (GO:0050793)	2673	13	2.56	+	5.07	8.29E-08	2.23E-05
negative regulation of gene expression (GO:0010629)	2065	10	1.98	+	5.05	6.68E-06	9.84E-04
gene expression (GO:0010467)	2109	10	2.02	+	4.94	8.07E-06	1.15E-03
macromolecule biosynthetic process (GO:0009059)	1689	8	1.62	+	4.94	9.72E-05	9.10E-03
regulation of RNA metabolic process (GO:0051252)	3809	18	3.65	+	4.93	6.91E-12	7.85E-09

positive regulation of macromolecule metabolic process (GO:0010604)	3630	17	3.48	+	4.88	8.52E-11	5.89E-08			
cellular response to organic substance (GO:0071310)	2368	11	2.27	+	4.84	2.59E-06	4.34E-04			
response to organic substance (GO:0010033)	3032	14	2.91	+	4.81	3.14E-08	1.02E-05			
regulation of cellular macromolecule biosynthetic process (GO:2000112)	3924	18	3.76	+	4.78	1.16E-11	1.23E-08			
regulation of apoptotic process (GO:0042981)	1566	7	1.50	+	4.66	4.40E-04	3.15E-02			
regulation of macromolecule biosynthetic process (GO:0010556)	4032	18	3.87	+	4.65	1.87E-11	1.65E-08			
regulation of nucleobase-containing compound metabolic process (GO:0019219)	4078	18	3.91	+	4.60	2.28E-11	1.91E-08			
regulation of programmed cell death (GO:0043067)	1588	7	1.52	+	4.60	4.79E-04	3.37E-02			
generation of neurons (GO:0048699)	1599	7	1.53	+	4.56	4.99E-04	3.48E-02			
positive regulation of metabolic process (GO:0009893)	3937	17	3.78	+	4.50	3.21E-10	2.04E-07			
regulation of cellular biosynthetic process (GO:0031326)	4184	18	4.01	+	4.49	3.58E-11	2.84E-08			
animal organ development (GO:0048513)	3277	14	3.14	+	4.45	8.61E-08	2.28E-05			
regulation of response to stress (GO:0080134)	1641	7	1.57	+	4.45	5.84E-04	4.02E-02			
regulation of biosynthetic process (GO:0009889)	4270	18	4.10	+	4.39	5.10E-11	3.69E-08			
neurogenesis (GO:0022008)	1703	7	1.63	+	4.29	7.30E-04	4.84E-02			
cellular response to chemical stimulus (GO:0070887)	2941	12	2.82	+	4.25	2.62E-06	4.34E-04			
anatomical structure morphogenesis (GO:0009653)	2206	9	2.12	+	4.25	9.47E-05	8.96E-03			
nucleobase-containing compound metabolic process (GO:0006139)	2740	11	2.63	+	4.19	1.09E-05	1.46E-03			
negative regulation of nitrogen compound metabolic process (GO:0051172)	2497	10	2.40	+	4.18	3.61E-05	4.08E-03			
regulation of multicellular organismal process (GO:0051239)	3248	13	3.12	+	4.17	8.45E-07	1.60E-04			
cell differentiation (GO:0030154)	3788	15	3.63	+	4.13	4.84E-08	1.43E-05			
cellular developmental process (GO:0048869)	3845	15	3.69	+	4.07	5.96E-08	1.72E-05			
immune system process (GO:0002376)	2853	11	2.74	+	4.02	1.62E-05	2.04E-03			
heterocycle metabolic process (GO:0046483)	2936	11	2.82	+	3.91	2.13E-05	2.65E-03			
negative regulation of cellular metabolic process (GO:0031324)	2700	10	2.59	+	3.86	7.14E-05	7.01E-03			
nervous system development (GO:0007399)	2437	9	2.34	+	3.85	2.05E-04	1.71E-02			
cellular aromatic compound metabolic process (GO:0006725)	2986	11	2.86	+	3.84	2.51E-05	3.02E-03			
regulation of gene expression (GO:0010468)	4913	18	4.71	+	3.82	5.89E-10	3.60E-07			
organic cyclic compound metabolic process (GO:1901360)	3218	11	3.09	+	3.56	5.14E-05	5.34E-03			
negative regulation of macromolecule metabolic process (GO:0010605)	2951	10	2.83	+	3.53	1.53E-04	1.34E-02			
cellular nitrogen compound metabolic process (GO:0034641)	3401	11	3.26	+	3.37	8.67E-05	8.41E-03			
response to chemical (GO:0042221)	4417	14	4.24	+	3.30	3.86E-06	6.14E-04			
regulation of signal transduction (GO:0009966)	3174	10	3.04	+	3.28	2.84E-04	2.23E-02			
negative regulation of metabolic process (GO:0009892)	3205	10	3.07	+	3.25	3.08E-04	2.35E-02			
system development (GO:0048731)	4525	14	4.34	+	3.23	5.22E-06	7.91E-04			
regulation of nitrogen compound metabolic process (GO:0051171)	5920	18	5.68	+	3.17	1.49E-08	5.92E-06			
negative regulation of cellular process (GO:0048523)	4981	15	4.78	+	3.14	2.09E-06	3.58E-04			
positive regulation of cellular process (GO:0048522)	5742	17	5.51	+	3.09	1.42E-07	3.27E-05			
regulation of response to stimulus (GO:0048583)	4404	13	4.22	+	3.08	2.85E-05	3.39E-03			
regulation of primary metabolic process (GO:0080090)	6118	18	5.87	+	3.07	2.62E-08	9.70E-06			
regulation of cellular metabolic process (GO:0031323)	6329	18	6.07	+	2.97	4.69E-08	1.41E-05			
regulation of macromolecule metabolic process (GO:0060255)	6510	18	6.24	+	2.88	7.61E-08	2.09E-05			
multicellular organism development (GO:0007275)	5106	14	4.90	+	2.86	2.32E-05	2.84E-03			
positive regulation of biological process (GO:0048518)	6347	17	6.09	+	2.79	6.93E-07	1.36E-04			
negative regulation of biological process (GO:0048519)	5643	15	5.41	+	2.77	1.12E-05	1.48E-03			
anatomical structure development (GO:0048856)	5489	14	5.26	+	2.66	5.58E-05	5.69E-03			
regulation of metabolic process (GO:0019222)	7060	18	6.77	+	2.66	3.04E-07	6.46E-05			
developmental process (GO:0032502)	5941	15	5.70	+	2.63	2.21E-05	2.72E-03			
multicellular organismal process (GO:0032501)	7148	15	6.86	+	2.19	2.41E-04	1.95E-02			
regulation of cellular process (GO:0050794)	11390	19	10.93	+	1.74	1.39E-04	1.25E-02			
regulation of biological process (GO:0050789)	11955	19	11.47	+	1.66	3.58E-04	2.65E-02			